AN EXPERIMENTAL STUDY OF COLLISION BROADENING OF SOME EXCITED ROTATIONAL STATES OF THE BENDING VIBRATION OF METHYL CYANIDE

DISSERTATION

Presented to the Graduate Council of the
University of North Texas in Partial
Fulfillment of the Requirements

For the Degree of
DOCTOR OF PHILOSOPHY

By

Jamal Y. Hajsaleh, B. S., M. S.
Denton, Texas

May, 1993

AN EXPERIMENTAL STUDY OF COLLISION BROADENING OF SOME EXCITED ROTATIONAL STATES OF THE BENDING VIBRATION OF METHYL CYANIDE

DISSERTATION

Presented to the Graduate Council of the
University of North Texas in Partial
Fulfillment of the Requirements

For the Degree of
DOCTOR OF PHILOSOPHY

By

Jamal Y. Hajsaleh, B. S., M. S.
Denton, Texas

May, 1993

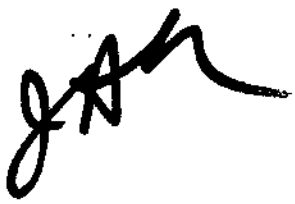

Hajsaleh, Jamal Y., An Experimental Study of Collision Broadening of Some Excited Rotational States of The Bending Vibration of Methyl Cyanide, Doctor of Philosophy (Physics), May, 1993, 109 pp., 4 tables, 22 illustration, bibliography, 69 titles.

A double modulation microwave spectrometer is used to evaluate the linewidth parameters for some excited rotational components in the bending vibration ν_8 of $^{13}CH_3{}^{13}C^{15}N$ and $^{13}CH_3C^{15}N$ isotopomers of methyl cyanide. The linewidth parameters for self-broadening of the $\Delta J=2\leftarrow1$ rotational components for the ground ν_8 , $1\nu_8$, and the $2\nu_8$ vibrations were determined over a pressure range of 1 to 13 mtorr and at a temperature of 300 K.

The double modulation technique is used to explore the high eighth derivative of the line shape profile of the spectral line. This technique proved to give good signal-to-noise ratios and enabled the recovery of weak signals. An experimental method is developed to correct for source modulation broadening. The tests of the ratios of the two inner peak's separation of the eighth derivative of the line showed that they were up to 95% similar to those for a Lorentzian line shape function. The line shapes were assumed to be Lorentzian for the theoretical analysis of the derivative profiles and comparisons were made between

experiment and theory on this basis.

Dipole moments for vibrationally excited states were calculated from linewidth parameters and show systematic decrease with the increase of excitation. Impact parameters were calculated using the "hard sphere" model of the kinetic theory of gases. The results were many times larger than the size of the molecule itself. This suggests that the dominant interaction is a long range dipole-dipole force interaction.

TABLE OF CONTENTS

TABLES OF CONTENTS - continued

LIST OF TABLES

TABLE

LIST OF ILLUSTRATIONS

Figure

LIST OF ILLUSTRATIONS-continued

Figure

LIST OF ILLUSTRATIONS-continued

Figure

Figure

CHAPTER I

INTRODUCTION

Molecular spectroscopy plays a major role in inquiring into molecular systems, especially in the gaseous phase. It is also a dependable method that produces more details and information about the structure and the properties of individual molecules. A basic experiment consists of three parts: radiation source, target cell, and a detection system. Radiation in a well known range of frequencies is selected to interact with the target gas, the outcome of the interaction is detected and then analyzed.

The kind of study and the molecular system of interest determine the type of spectroscopy to be used. For frequency ranges corresponding to transitions of rotational states of symmetric top molecules, where the allowed transitions between these states yield a well defined set of rotational spectral lines, microwave spectroscopy is the appropriate type. The high precision measurement of spectral lines in microwave spectroscopy is one of its important characteristics. In some cases, this precision is on the order of a few Khz[1] out of a few Ghz. Another important characteristic is the narrowness of these lines; their widths usually are on the order of 10^{-4} to 10^{-6} of the

line center frequency[2]. The width of the spectral line is of interest since the width is a measure of the molecular environment and it is subjected to different circumstances even for the same line. This feature of spectral lines has received wide experimental and theoretical interest[3].

The width of the line can be thought of in terms of the uncertainty principle. Consider a transition between two energy levels E_1 and E_2. The transition time, Δt, is associated with some uncertainty in these levels. From the uncertainty relation, $\Delta E \Delta t \approx \hbar$, the energy levels E_1 and E_2 become ΔE_1 and ΔE_2. The transition then, is between two ranges of levels, and the result is a band of energies with $|E_1 - E_2|$ being the most probable value and this energy difference gives the center peak for a such transition. A schematic illustration is given in figure 1. This picture, however, is not completely accurate. The contribution of the uncertainty spread in energy, usually called the natural breadth, is infinitesimal and considered the least effective source of the width broadening compared with other sources.

Traditionally, spectral line broadening sources are: natural breadth, Doppler effect, saturation effect, cell length, pressure, source modulation and overlapping lines. Each source has its own parameters that determine its contribution. The linewidth is simply the sum of all of the contributions. The importance of line broadening sources depends on how much each affects the width of the line.

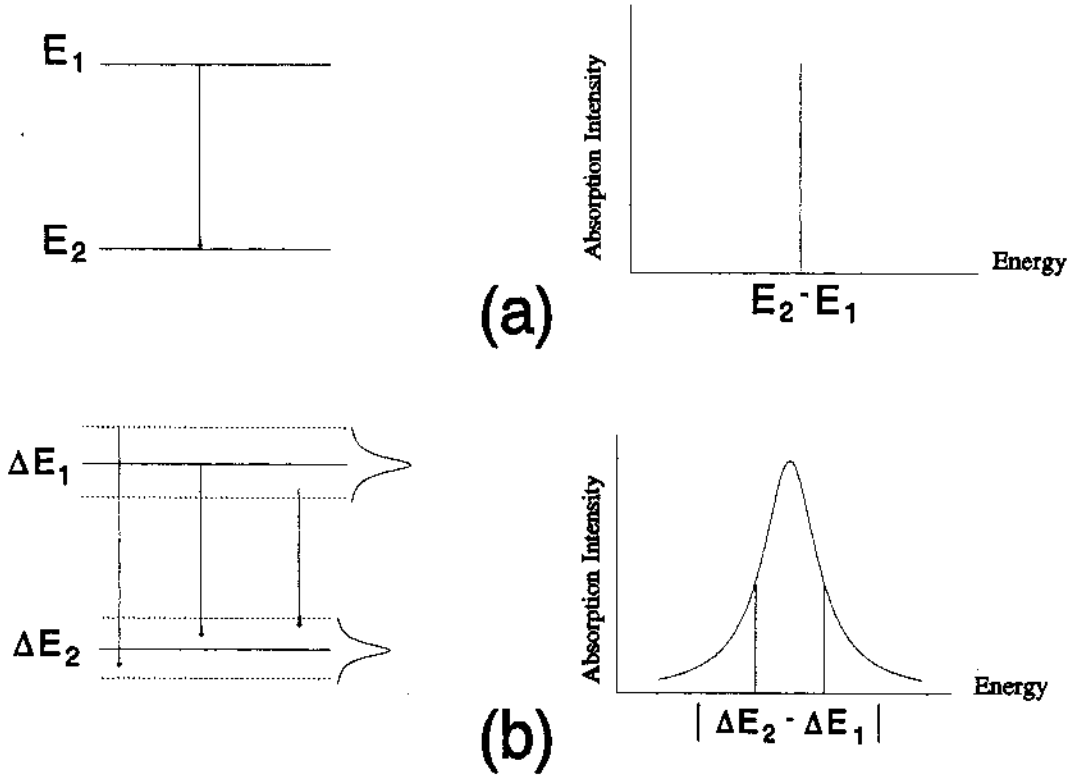

Figure 1. A schematic illustration of an energy transition spectrum profile between: (a) two well-defined states and (b) two energy ranges.

Natural breadth is very small and negligible in almost all cases. The Doppler effect is much larger but still has a small contribution to the width; however, it is an important factor at low pressures. The power saturation effect and the cell length effect can be controlled and minimized experimentally. Source modulation depends on the modulation amplitude and for large amplitudes, correction factors have to be made. To deal with overlapping spectral lines overlapping is difficult and requires special treatment. The most important source of all linewidth is the pressure width. Since the influence of pressure is the dominant effect, and reflects the dynamics of the molecular system, a great deal of information can be obtained by examining the details of the broadening of the linewidth due to pressure. Theoretical treatment of these sources are given in the next chapter.

Methyl cyanide, CH_3CN, also called acetonitrile, used in this work is a symmetric top molecule with the principle axis of rotation along the C-C≡N bonds. It is an abundant species in interstellar space and on some minor satellites. Exploring the molecular behavior of this molecule is necessary to better comprehend the nature of momentum and energy transfer in involving this chemical species. This information is very important also in understanding atmospheric canopies of such planets[4].

The methyl cyanide molecule has eight fundamental

vibrational modes[5] as described in Table I. The ν_8 vibration represents the bending of the Nitrogen-Carbon bonds along the symmetric axis[6] as shown in figure 2. Methyl cyanide's large dipole moment and good vapor pressure at room temperature make it an ideal target for microwave spectroscopy.

While structure studies of the molecule have been extensively reported by a number of authors[7-17], linewidth studies have been limited to the ground state and to specific problems. Roberts et al[18] included methyl cyanide in a study of linewidth parameters of symmetrical tops and reported a high linewidth parameter (100 Mhz/torr) for the rotational transition of $\Delta J=0\rightarrow1$ and $K=0$ in methyl cyanide. Broadening due to collision with other molecules ($CH_3{}^{81}Br$-CH_3CN) based on dipole-dipole interaction theory was investigated by Johri et al[19]. The temperature effect, which was found to be minor in line width broadening, was reported by Swindle et al[20] and Johri et al[21]. Messer and Roberts[22] studied the spectral lines overlapping effect and Story et al[23] measured the line shift due to pressure.

In this work, pressure broadening of spectral lines is used to calculate the line width parameter, $\Delta\nu_p$, of the bending vibration, ν_8, in the first and second excited states of methyl cyanide. The isotopomers $^{13}CH_3{}^{12}C^{15}N$ and $^{13}CH_3{}^{13}C^{15}N$ were examined in this investigation. $\Delta\nu_p$ was used to calculate the dipole moment, μ, and the cross-section, σ,

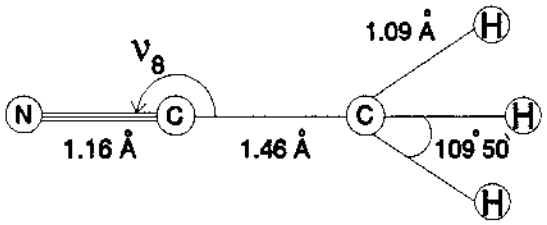

Figure 2. Methyl cyanide molecular structure. (obtained from reference 6)

VIBRATION	DESIGNATED MOTION
ν_1	C-H Stretching
ν_2	C≡N Stretching
ν_3	CH_3 Deformation
ν_4	C-C Stretching
ν_5	Antisymmetric CH_3 Stretching
ν_6	Antisymmetrical Deformation of the three C-C-H angles
ν_7	CH_3 Rocking
ν_8	C-C≡N Bending

Table I. A summary of the vibrational states of the methyl cyanide molecule. (table taken from reference 5)

for these states. The line width was measured as the pressure varied over the pressure range between 1 to 13 mtorr.

The change in the molecular structure when vibrational modes are excited will change various parameters, especially the dipole moment. Dipole moment calculation is very important in constructing a theoretical model of the molecular system. The importance results from the fact that rotational spectra are the results of the dipole moment's presence. Except in rare cases, for non-polar molecules, no rotational spectra are observed if the dipole moment is zero, since the spectral intensities are proportional to the square of the dipole moment matrix element.

Stark modulation, which is the conventional tool for dipole moment measurements, is reliable only in the ground states where the number of spectral lines is small and their intensities are high. For excited states, this is not the case. The intensities of these lines, which are low initially, are reduced even further with the application of the Stark field. The application of the field also introduces perturbation of the energy levels that is large compared to the difference between these energy levels. In other words, the applied field will broaden these states and the experimental measurements will be very difficult if not impossible to realize.

The linewidth parameter method of calculating the

dipole moment is the first of its kind for methyl cyanide. For weak lines such as those of the ν_8 excited states considered, the pressure broadening is the only reliable method, reported to date, that can be used to measure them effectively.

The molecular collision cross-section is related to the linewidth parameter through the mean time, τ, between collisions. Once the cross-section, σ, is calculated, the impact parameter, b, can be evaluated and a clearer picture of the molecules behavior is obtained. The hard sphere collision model of the kinetic theory of gases is used to derive the necessary equations to perform the calculations on cross-sections.

The pressure broadening method is an alternative technique for the calculation of μ (the dipole moment) and σ (the cross-section) of these states, given that the lines are well resolved. An important goal of this experiment is the measurement of the linewidth of the spectral lines of some weak vibrational states over a range of pressures so that $\Delta\nu_p$ can be calculated. To achieve good and reliable measurements of the linewidth parameter of these weak states, the derivative technique is used, with some modification. A new eighth derivative approach is used and proven to fulfill the goal of obtaining good spectral line resolution and proven to be effective in reducing the effect of the standing waves on the lines. Also, the good signal-

to-noise ratio obtained enabled the taking of the data with high accuracy, even for some weak lines.

In Chapter II, a general discussion of the line shape and the Lorentz theory of line shapes is given. It was assumed that the lines should have Lorentzian shape and the departures from this shape were assumed to be due to factors other than the pressure broadening. Contribution to the line width from these factors is then discussed briefly according to their importance. Detailed derivations are given when necessary. Corrections to the line width are derived and are given to assist in the analysis of the measurements and the calculations.

In Chapter III, the pressure broadening theory is given in more detail. A review and discussion of the impact theory of Anderson which proved to be more successful in the range of the pressure considered in the work is given. Major emphasis was given to Anderson's results in calculating the dipole moments and the collision impact parameter. Corrections to the model by Murphy and Boggs are also outlined.

In Chapter IV, the spectrometer is discussed. Its description is subdivided into three parts according to the role of operation, and each part is discussed in light of the effect of its various parameters. The derivative technique is discussed in further detail. The data measurements and their analysis are discussed in Chapter V.

A summary of the results and discussion of the errors and the limitation of the investigation is also given.

In Chapter VI, the main conclusions and results of the investigation are given. A complete picture of the mechanism of the collision process is obtained. The comparison of the results with other investigations is also presented.

CHAPTER II

LINE SHAPE AND BROADENING SOURCES

A stationary molecular system has fixed and defined energy levels. The transition between any two states can be detected and appears as a spectral line. The shape of the line is similar to a normal distribution function with the bell peak representing the transition energy, or frequency, of the transition between the two states. The half width at half maximum is called the line width $\Delta\nu$. Figure 3 shows a schematic diagram of a spectral line with the parameters of interest noted.

The line width, $\Delta\nu$, represents the perturbation in the energy levels because of various sources. The most important one for the case of molecules in the gas state is the pressure. The pressure is a measure of the interaction between molecules and, thus, its effect on the line width is essential in the study of the energy transfer and the dynamics of the molecules. Other sources are also important in correcting the experimental results in order to fit the theoretical model.

Collision broadening theories started with Debye[24]. He proposed a theory in which he used a theory of dispersion to formulate a spectral model. Debye's model considers only

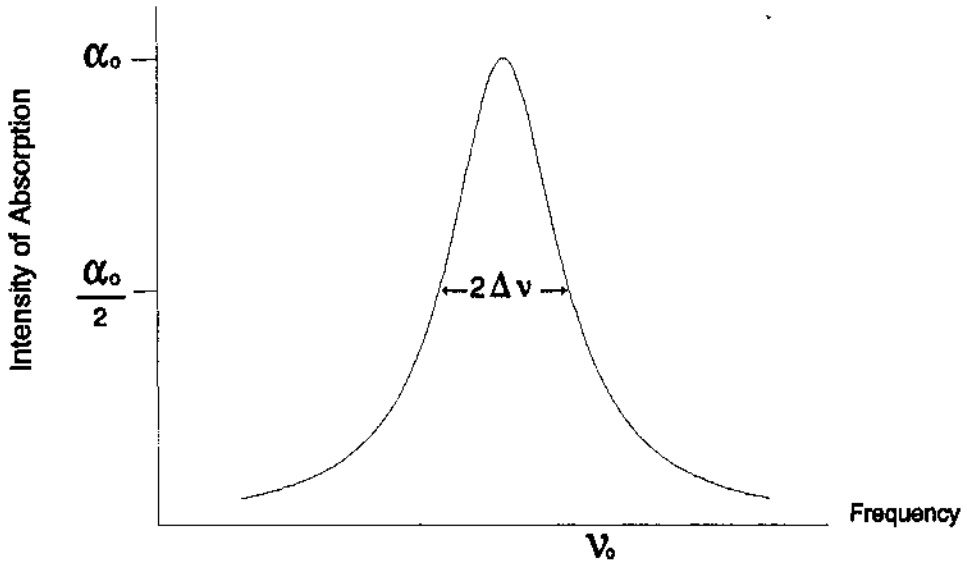

Figure 3. A spectral line profile. The frequency at the maximum absorption is the center frequency ν_o and the width at half-maximum is $2\Delta\nu$.

"weak" collisions of a large number of molecules, and thusis useful primarily for non-resonant lines. The term weak means that individual collisions have little effect in disturbing the pre-collision orientation and polarization of the molecules. Since the disturbances are very small, large number of collisions are required to result in an appreciable change in the distributions. The model is classified under the statistical theories of collision broadening.

Other models are classified under the impact theories[25]. The basis of these theories is the work of Lorentz[26] which considers solving the equation of motion of a harmonic oscillator under an incident radiation. Van Vleck and Weisskopf[27] argued that Lorentz's absorption formula does not reduce to Debye's for non-resonant lines, which can be considered special cases of resonant lines with the frequency equal to zero. The correction that was proposed was to use different boundary conditions from those used by Lorentz. Instead of an unpolarized mean distribution after collisions, which was assumed by Lorentz, the polarization according to Boltzmann statistics was applied. This corrected model proved to work in removing the discrepancy in Lorentz's model. The absorption coefficient formula in the corrected model (see Appendix A) can be written as:

$$\alpha = \frac{8\pi^2 Nf}{3ckT} |\mu_{ij}|^2 \nu^2 \left[\frac{\Delta\nu}{(\nu-\nu_o)^2+(\Delta\nu)^2} + \frac{\Delta\nu}{(\nu+\nu_o)^2+(\Delta\nu)^2} \right], \qquad (1)$$

where N is the number of molecules per unit volume, c is the speed of light, k is the Boltzmann constant, T is the absolute temperature, ν_0 is the line center frequency, $\Delta\nu$ is the spread in frequency, $|\mu_{ij}|^2$ is the dipole moment matrix element, f is the fraction of molecules in the lower energy state, and $\Delta\nu$ is the absorption half width at half maximum. At low pressures where $\Delta\nu \ll \nu_o$, the second term in Eq. (1) vanishes and it reduces to:

$$\alpha = \frac{8\pi^2 Nf}{3ckT} |\mu_{ij}|^2 \nu^2 \left[\frac{\Delta\nu}{(\nu-\nu_o)^2+(\Delta\nu)^2}\right]. \qquad (2)$$

Among all parameters in Eq. (2), it is useful to define the part which controls the shape of the line. This part, which is called the line shape factor, can be written as:

$$F(\nu) = \frac{1}{(\nu-\nu_o)^2 + (\Delta\nu)^2}. \qquad (3)$$

The function gives the same shape as observed for experimental spectral lines and thus, it is customary to say that these lines have a "Lorentzian shape".

If the line shape is assumed to be Lorentzian, then the shape factor can be used to assist in experimental width measurements. Eq. (3) can be put in a more manageable form by replacing $(\nu-\nu_o)/\Delta\nu$ by x. The new form then is:

$$F(\nu) = constant \frac{1}{(x)^2 + 1}, \qquad (4)$$

The line shape function and any of its derivatives can

now be obtained for the spectral line sought. The theoretical derivative is obtained in a straight forward way by taking the desired order of the derivative of Eq. (4). The experimental line derivative profile is obtained by the technique outlined later. The eighth derivative was chosen in this work as it gave good signal-to-noise ratios. The corresponding function is:

$$F^{(8)}(x) = constant\,[1-36x^2+126x^4-84x^6+9x^8]\,[1+x^2]^{-9}. \qquad (5)$$

Derivatives of Eq. (4) up to the ninth order are given in Appendix B.

In determining the line width, one needs only the critical points of the function derivative. For the eighth derivative profile, the critical points are obtained by taking the roots of the ninth derivative in the standard way. Figure 4 shows the eighth derivative compared with the original function. The eighth derivative has the critical points located from the center at 0, ±0.3249, ±0.7265, ±1.3764, and ±3.0777 times the half width at half power maximum, respectively. These spacing, within the experimental error, were found to hold for the inner two separations distances of the spectral lines. The ratios of the inner separations to the original function were then used to determine the measured half width at half power separation. The measured half width of a spectral line, $\delta\nu$, is obtained by

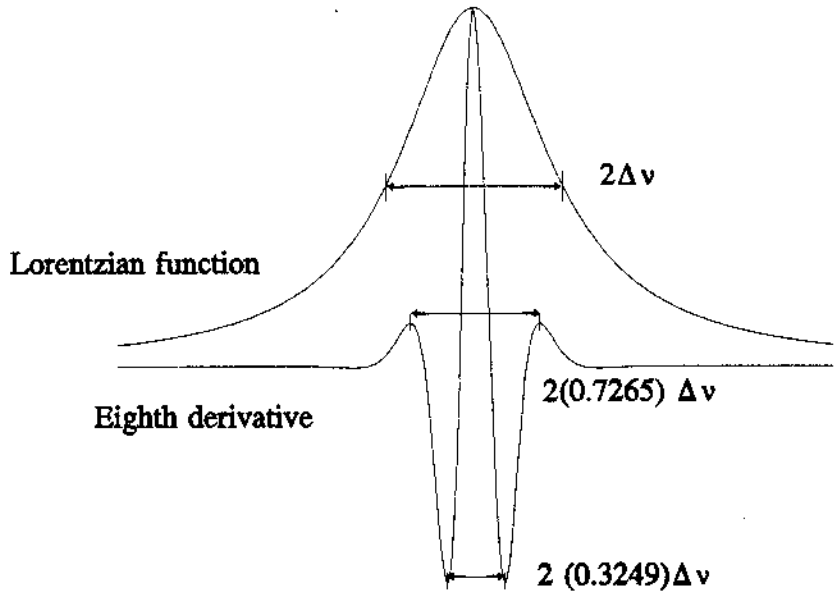

Figure 4. The eighth derivative of a Lorentzian shape function with critical points are compared with the original function.

$$\delta\nu = \frac{1}{\sqrt{1-\sqrt{0.8}}} \times \textit{Inner peak distance.} \qquad (6)$$

and

$$\delta\nu = \sqrt{1+\sqrt{0.8}} \times \textit{Next inner peak distance.} \qquad (7)$$

The experimental results proved that the detected lines were Lorentzian. This was shown by taking the ratio of peak spacing from experimental data and comparing this to those spacing predicted for a Lorentzian shape line. Figure 5 shows a dual-pen chart recorder scan of the $\Delta J=2\leftarrow1$ spectra for (K=0, ℓ=2), (K=0, ℓ=0), (K=1, ℓ=0), and (K=-1, ℓ=2) in the $2\nu_8$ vibrational levels of the $^{13}CH_3{}^{13}C^{15}N$ isotopomer. Scan (a) is the chart recorder with markers and scan (b) is a computer generated profile of a theoretical output for the same lines using Lorentzian functions. The agreement between the theoretical and the experimental outputs shows the assumption that the lines are Lorentzian shape is a valid one.

Some differences between the two scans are expected since the line shape is distorted by modulation broadening, Doppler broadening, cell length (differential saturation), and wall broadening in addition to some standing waves. In order to compare the agreement between the theoretical model

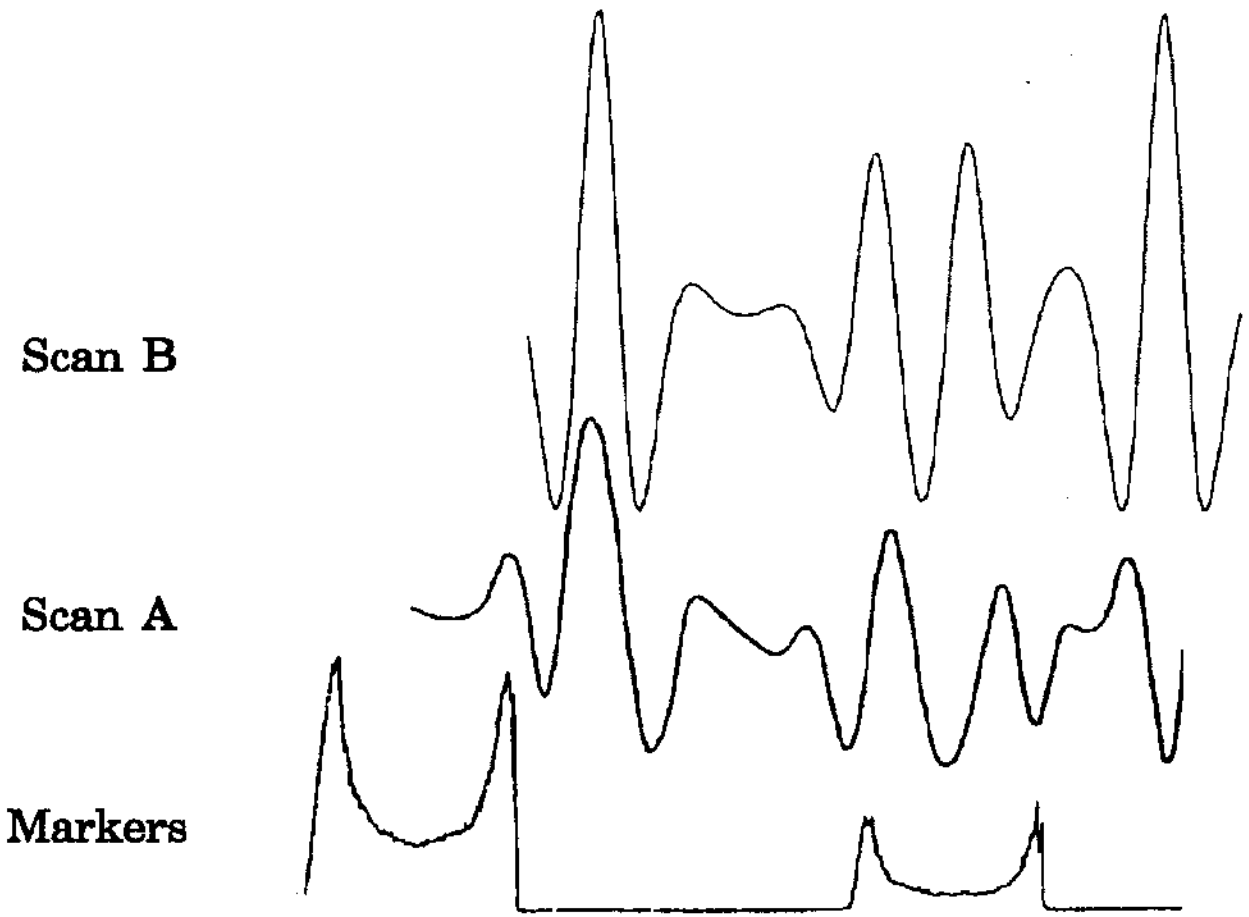

Figure 5. A dual-pen chart recorder scan of the $\Delta J=2\leftarrow1$ spectra for four lines in the $2\nu_8$ vibrational level. Scan A is the experimental output and scan B is the theoretical model four Lorentzian shape lines of assumed theoretical intensities and measured frequency spacings.

and the experiment, corrections due to other sources have to be made and this was done before μ and σ were calculated.

Disturbances of energy levels due to different sources vary. In the following sections, a discussion of each source is briefly presented and derivation are given when necessary. Sources of contribution to the linewidth are:

1. Natural Breadth.
2. Wall Broadening.
3. Saturation Broadening.
4. Source Modulation.
5. Spectral lines Overlapping.
6. Doppler Effect.
7. Pressure broadening.

Broadening due to standing waves was not discussed since it depends on the geometry of the cell and the frequency of the radiation, so its contribution can be minimized by the spectrometer adjustments. Adjustments were basically in minimizing the power reflections in the spectrometer elements and in using the eighth order of the derivative technique. This technique reduces the baseline and increase the signal-to-nise ratio. Standing waves also do not, generally, follow a systematic pattern, and thus has no theoretical model for it has been derived.

1.Natural Breadth

This broadening results from the zero-point vibrations of electromagnetic fields that are always present in the free space. For a spontaneous transition of frequency ν from an excited state to the ground state, the probability for the process is[28]:

$$P = \frac{1}{\Delta t} = \frac{64\pi^4}{3hc^3} |\mu|^2, \tag{8}$$

where Δt is the lifetime of the excited state. The spread in the energy, ΔE, is related to Δt by the uncertainty relation:

$$\Delta E \, \Delta t \approx \hbar. \tag{9}$$

Rewriting ΔE as $h\Delta\nu$ and substituting Eq. (8) in Eq. (9), the spread in frequency is:

$$\Delta \nu = \frac{32\pi^3}{3hc^3} \nu^3 |\mu|^2. \tag{10}$$

For methyl cyanide, the dipole moment is 3.92 debye[29] ($1D=10^{-18}$ esu) and for the ν_8 levels of 17 and 34 GHz, the frequency spreads are on the order of 10^{-7} and 10^{-6} Hz, respectively. This spread is completely negligible compared with other sources of spreading. The natural breadth, however, is enhanced a great deal by fields generated in the cell due to thermal motions of electrons. These fields have mean energies of kT rather than those of zero-point fields

which have mean energies of ½ hν. At room temperature the ratio of the two for methyl cyanide is about 700 times larger for kT. Nevertheless, the effect is negligibly small.

2. Wall Broadening

The collisions between the molecules and the walls of the absorption cell alter the process of absorption. The broadening of such collisions, in general, can be treated using the kinetic theory of gases. The frequency spread is given by[30]:

$$\Delta\nu = \frac{A}{V}\sqrt{\frac{RT}{8\pi^3 M}}, \tag{11}$$

where R is the gas constant, M is the molecular weight, A and V are the total area and volume of the cell, respectively. A more specific model for circular cells was derived by Danos and Geschwind[31] in which the frequency spread can be calculated according to:

$$\Delta\nu = \frac{1.25}{4\pi r}\sqrt{\frac{2kT}{m}}, \tag{12}$$

where r is the cell radius, k is Boltzmann's constant, and m is the mass of each molecule. Whichever model is used, the contribution to the line breadth for methyl cyanide in the cell used in this work is less than 2 Khz. This amount is

too small to be significant and thus, like the natural breadth, can be ignored. Also, the contribution is independent of pressure and thus, the slope of linewidth versus the pressure is not altered.

3. Saturation Broadening

High power radiation in the cell increases the lifetime of the excited states, and the transition among the molecular states are induced at a rate that is not negligible compared with the collision rate. This process violates the thermal equilibrium and broadens the spectral lines. The power saturation has another effect on the line shape, and that is the reduction of the intensity of the absorption. The saturation treatment has been worked on by many authors[32-35] and it has been experimentally observed[36]. The saturation has been reported to occur for methyl cyanide at power levels as low as 1 milliwatt per cm^2. The effect was avoided in this work by using lower power levels.

4. Source Modulation

The radiation output frequency is sinusoidally modulated, since the voltage applied to the klystron was modulated by a sine wave. This modulation allows a step-by-step sampling of the absorption line. In this sampling, a

chopper circuit is used to sweep the frequency back and forth between successive points on the resonance in that part of the over all sweep. The output of this chopping at any instant is the frequency difference between any two successive points of that instant divided by their sweep increment. As illustrated in figure 6, for any two points A and B the output is:

$$OUTPUT = \frac{f(B) - f(A)}{B - A}, \tag{13}$$

By substitution of the independent variable and minimizing the increment between the two points this equation becomes:

$$OUTPUT = \lim_{\Delta x \to 0} \frac{f(x+\Delta x) - f(x)}{\Delta x}. \tag{14}$$

This result is simply the definition of the derivative of f(x). Thus, the output corresponds to a derivative of the line profile.

The general theory for frequency modulation in microwave spectroscopy was first investigated by Karplus[37]. Modification to the theory was made by Rinehart et al[38] to apply it to low amplitude modulation in which the change of the source frequency over a period of modulation is less than the width of the spectral line. Higher amplitude modulation modifications were made by Netterfeild et al[39].

The theory predicts the line shape components occurring at a fundamental modulation frequency f and also at harmonics of f which are proportional to the higher

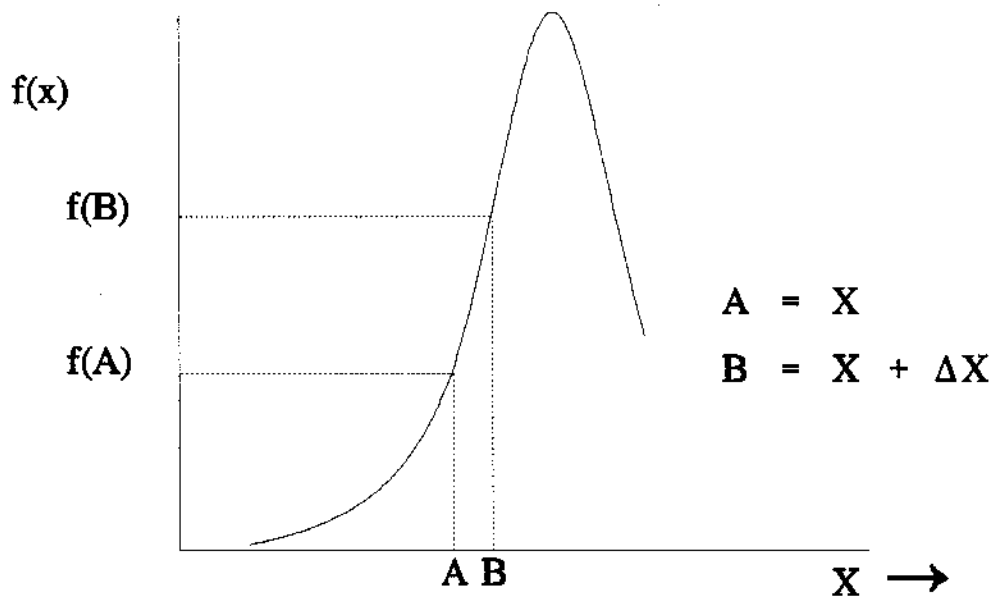

Figure 6. Mathematical illustration of a slow modulation which is equivalent to the derivative definition.

derivatives of the absorption line. If the modulation is f/n, the output from the amplifier will correspond to the nth derivative of the spectral line profile. This result is very useful and has been implemented as an experimental technique. The determination of critical points of the line derivative reduces the background contribution and thus can be related to the width calculation. This technique enhances the resolution of the measurements. The basic concept of the technique is the use of signal amplifying very narrow band-pass amplifiers with center frequency f and modulating the periodic voltage at f/n, where n is the derivative order. The result of this procedure is the display of the nth derivative instead the original line profile.

The modulation introduces broadening to the spectral lines and may lead to line overlapping for near lying lines as shown in figure 7 for $\Delta J=2\leftarrow1$, K=0 and K=1 components for the ground vibration of $^{13}CH_3{}^{13}C^{15}N$ isotopomer. This effect needs appropriate treatment to correct for measurements of the width. For slow modulation (i.e. $f<\frac{1}{2}\Delta\nu$), the correction for the first two derivatives can be written as:

$$\delta\nu_1 = \frac{\Delta\nu}{\sqrt{3}}\left[1 + \frac{1}{2}\left(\frac{f'}{\Delta\nu}\right)^2 + \frac{3}{4}\left(\frac{f}{\Delta\nu}\right)^2\right], \qquad (15)$$

and

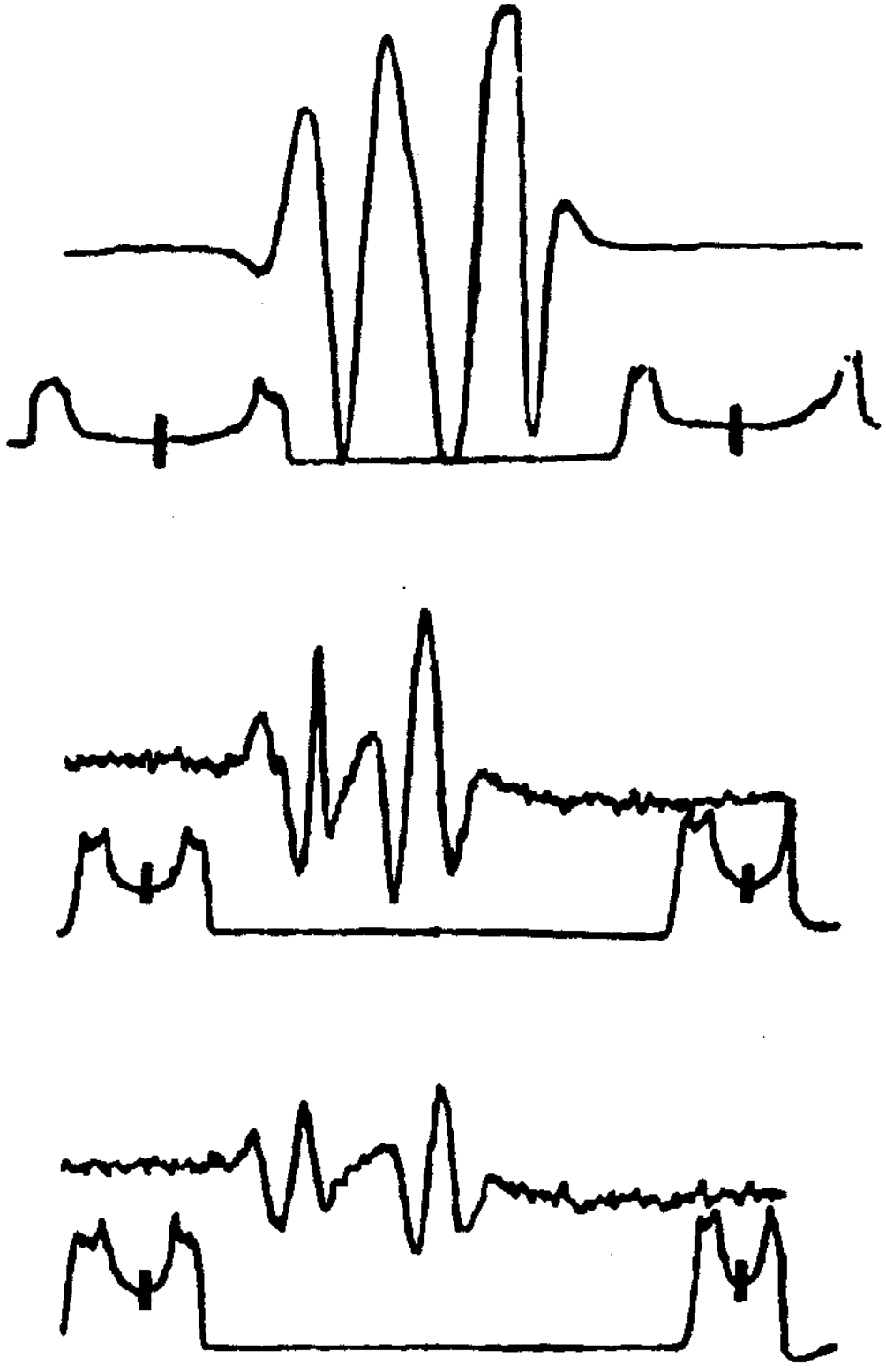

Figure 7. A dual-pen chart recorder scan of the $\Delta J=2\leftarrow1$, k=1 components for three levels of modulation.

$$\delta\nu_2 = \Delta\nu\left[1 + \frac{3}{16}\left(\frac{f'}{\Delta\nu}\right)^2 + \frac{1}{2}\left(\frac{f}{\Delta\nu}\right)^2\right], \quad (16)$$

where $\delta\nu_{1,2}$ is the measured width of the first and second derivatives, respectively, $\Delta\nu$ is the true width, f' is the modulation amplitude, and f is the modulation frequency.

The theoretical expressions derived for modulation are subject to approximations which cannot be satisfied in the experimental arrangement and maintain well-defined signals. To overcome this problem, an experimental model to correct for the eighth derivative due to modulation was produced. This was done in the following way: A spectral line was measured after the pressure had stabilized, over a wide range of modulation amplitudes and each line width and modulation amplitude were recorded. A plot was then made of the line width versus modulation amplitude. The "best-fit" curve through the data served as a correction model for modulation correction as the width was changed due to pressure. For modulation levels employed, the measured width $\delta\nu$ of the data, within experimental error, could be fitted to an equation of the form:

$$\delta\nu = M\left(\frac{f'}{\Delta\nu}\right)^2 + C, \quad (17)$$

where M is the slope of the assumed straight line plot of $\delta\nu$ versus modulation amplitudes. The residual c includes the line width $\Delta\nu$ and another term in the modulation correction

formula $\frac{1}{2}[(f/n)/\Delta\nu]^2$ due to the frequency of the modulation signal. Therefore, $\Delta\nu$ can be obtained from the equation:

$$\Delta\nu = \delta\nu - M\left(\frac{f'}{\delta\nu}\right)^2 - \frac{1}{2}\left(\frac{f/n}{\Delta\nu}\right)^2, \tag{18}$$

where f/n is the modulation frequency of the periodic voltage. The value f' is obtained by measuring the frequency splitting, the klystron excursion frequency, of each frequency marker. Equation (18) fulfills the case when there is no modulation, since it reduces to $\Delta\nu = \delta\nu$.

5. Spectral lines overlapping

When two or more center frequencies are close enough, their profiles overlap and if the resolution of the spectrometer is not high enough, these profiles will appear to be a distorted profile of one line. The problem can be resolved only by enhancing the resolution of the spectrometer. Even though decreasing the pressure will, sometimes, resolve these lines, it is not, however, an acceptable solution since the topic of the work is the measurement of the line width over a range of pressures and not just frequency measurements.

For a composite line, the total width is related to the individual line width in a manner which depends on the spacing of the component lines as well as their relative

intensities. The line width measurement of such a composite line introduces a large departure from the Lorentzian model.

The effect of overlapping between lines was minimized in this work by the high resolution of the spectrometer. The measurements of linewidths of overlapping lines, whenever it occurred, were carefully dealt with by considering the spacings of the outer peaks, as will be addressed later.

6. Doppler Effect

Further broadening of the line is due to the Doppler effect. Random motions of the molecules with respect to the radiation cause a shift in the frequency perceived by the molecules. Consider a molecule moving in the cell with the field of radiation in the z-direction. The Doppler frequency shift in the longitudinal and the transverse directions, respectively, are given by[40]

$$\nu' = \nu \frac{1 \pm \frac{V_z}{C}}{\sqrt{1-\left(\frac{V_z}{C}\right)^2}}, \tag{19}$$

$$\nu'' = \nu \frac{1}{\sqrt{1-\left(\frac{V_t}{C}\right)^2}}, \tag{20}$$

where v_t is the tangential velocity. At room temperature,

the mean velocity of the molecules can be calculated by[41]

$$\overline{v} = \sqrt{\frac{8kT}{\pi m}}. \tag{21}$$

For methyl cyanide, this is on the order of 5.4×10^4 cm/s and the ratio of $(v/c)^2$ is about 3.4×10^{-12}, which is almost equal 2to zero compared with other terms and thus can be dropped. The shifts in both equations become

$$\nu'' = \nu, \tag{22}$$

$$\nu' = \nu \left[1 \pm \left(\frac{v_z}{c} \right) \right], \tag{23}$$

which means that the longitudinal shift is the only one appreciable for calculation. Now, for thermal equilibrium and dilute gases, the fraction of molecules per unit volume with velocities between **v** and **v**+d**v**, usually denoted by dN_v, can be written as[42]:

$$dN_v = \sqrt{\frac{m}{2\pi kT}}\, N_v\, e^{-\frac{mv^2}{2kT}}\, dv \tag{24}$$

or, for the same volume and the z-direction, it becomes:

$$dN = \sqrt{\frac{m}{2\pi kT}}\, N\, e^{-\frac{mv^2}{2kT}}\, dv_z. \tag{25}$$

Make the substitution from Eq. (21) for ν' and $d\nu'$ in terms of v_z and dv_z, respectively, to get,

$$dN = \sqrt{\frac{m}{2\pi kT}}\, N\, e^{-\frac{m}{2kT}\left(\frac{c}{\nu}\right)^2(\nu'-\nu)^2}\, \frac{c}{\nu}\, dv_z. \tag{26}$$

The absorption coefficient from Eq. (2) has the contribution of molecules in the z-direction

$$d\alpha = \frac{8\pi^2 f}{3ckT}\, |\mu_{ij}|^2\, \nu^2 \left[\frac{\Delta\nu}{(\nu-\nu_o)^2+(\Delta\nu)^2}\right] dN. \tag{27}$$

Substituting Eq. (25) into Eq. (26) gives

$$d\alpha = \frac{8\pi^2 f}{3ckT}\, |\mu_{ij}|^2\, \nu'^2 \left[\frac{\Delta\nu e^{-\frac{m}{2kT}\left(\frac{c}{\nu}\right)^2(\nu'-\nu)^2}}{(\nu'-\nu_o)^2+(\Delta\nu)^2}\right] \sqrt{\frac{m}{2\pi kT}}\, N\, \frac{c}{\nu}\, d\nu'. \tag{28}$$

This equation can be simplified by considering the effect to be strong in narrow lines, in which ν becomes approximately equal to ν_o and ν^2 can be substituted by ν_o^2 and by putting $\beta=(mc^2/2kT\nu_o^2)$ to get:

$$d\alpha = \frac{8\pi^2 f}{3ckT}\, |\mu_{ij}|^2\, \nu'^2 \left[\frac{\Delta\nu e^{-\beta(\nu'-\nu)^2}}{(\nu'-\nu_o)^2+(\Delta\nu)^2}\right] \sqrt{\frac{m}{2\pi kT}}\, N\, \frac{c}{\nu}\, d\nu'. \tag{29}$$

Combining the constants under A, the total contribution is:

$$\alpha = A\, N\, c\, \Delta\nu \int_{-\infty}^{\infty} \frac{\nu'^2}{\nu}\, \frac{e^{-\beta(\nu'-\nu)^2}}{(\nu'-\nu_o)^2+(\Delta\nu)^2}\, d\nu'. \tag{30}$$

For very localized lines, $\nu' \approx \nu$ and $\nu'^2/\nu = \nu \approx \nu_o$. When these replacements are made, Eq. (29) becomes:

$$\alpha = A\, N\, c\, \nu_o\, \Delta\nu \int_{-\infty}^{\infty} \frac{e^{-\beta(\nu'-\nu)^2}}{(\nu'-\nu_o)^2+(\Delta\nu)^2}\, d\nu'. \tag{31}$$

The absorption function in Eq. (30) clearly combines

the effects of collision broadening, which is represented by the Lorentzian term appearing in the denominator, and the Doppler broadening, which is represented by the Gaussian term appearing in the numerator.

Pressure broadening of such a heavy molecule with large dipole moment like methyl cyanide, is the dominant factor and thus, other factors can be calculated and used as correction factors. The Doppler effect factor was not under investigation and a rather simpler equation than (30) is used to calculate the correction instead. The correction can be calculated using[43]

$$\Delta \nu = 3.581 \times 10^{-7} \sqrt{\frac{T}{M}}\, \nu, \qquad (32)$$

where M is the molecular weight and ν is the radiation frequency. The broadening in Eq. (32) depends only on the mass of the sample molecules and the temperature. Using massive molecules at low temperature reduces the effect. For methyl cyanide, at room temperature, the ratio $\Delta\nu/\nu$ is about 10^{-6} which can be translated into 16 and 32 kHz for frequencies of 17 and 34 Ghz, respectively.

Pressure broadening, the last major source of broadening, is the one to be considered. The theory of collision broadening and the other parameters that can be obtained from it are discussed in detail in the next chapter.

CHAPTER III

PRESSURE BROADENING

Pressure is the dominant source of the broadening of spectral lines in the microwave region. This is clearly seen in figure 8 where a spectral line profile is recorded for different pressures. This broadening basically arises from molecular collisions. When two molecules are within each other's force field, the energy levels of both molecules will be perturbed. The broadening can be predicted from the uncertainty relation, $\Delta E \Delta t \approx \hbar$. Considering Δt to be the mean time between molecular collisions, τ, and writing the energy in terms of the frequency, the relation can be written as:

$$\Delta\nu = \frac{1}{2\pi\tau}. \tag{1}$$

For low pressures where binary collisions predominate, the kinetic theory of gases predicts that τ is inversely proportional to P and thus equation (1) leads to the proportionality relation:

$$\Delta\nu \propto P. \tag{2}$$

This relation suggests the linear relationship between the linewidth and the pressure. From this result, the pressure broadening studies can be used to provide information about

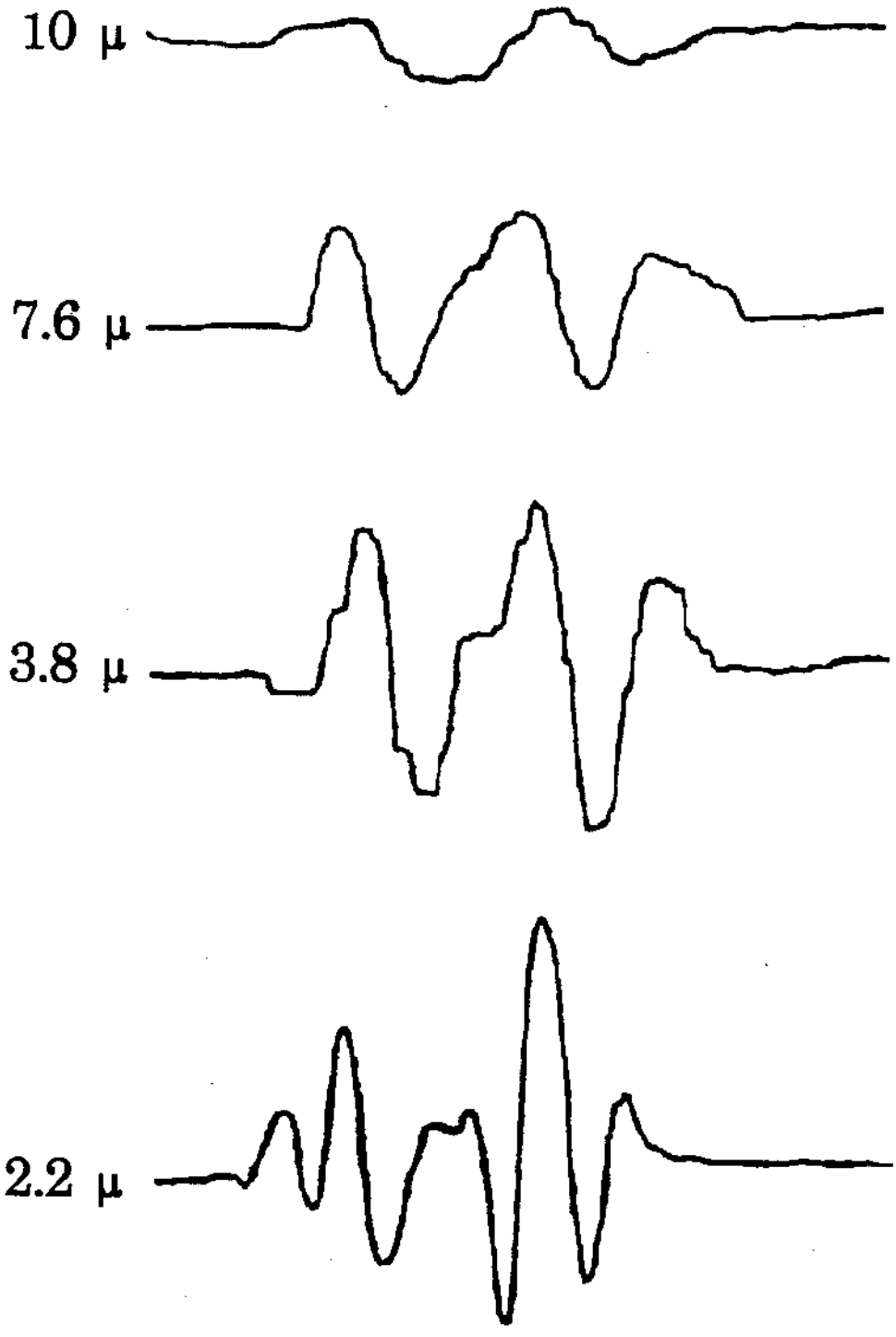

Figure 8. Profiles of a spectral line at different pressures.

how molecules behave in intermolecular collisions and hence better understand the nature of molecular force fields and the general behavior of the molecules during collisions.

Various molecular forces can be the cause of the broadening. These forces (dipole- dipole, dipole-quadruple, etc.) are generally proportional to r^{-n} where n is an integer corresponding to the order of the multipole. Only one or two force terms may be effective in the radius of interaction. Long range forces of collision are usually attributed to the broadening for polar species. In the case of methyl cyanide, the dipole-dipole interaction is so strong, because of its large dipole moment, that higher terms of interactions are not generally considered.

A comprehensive theory of pressure broadening which deals with a wide range of frequencies is does not exist since various interactions and parameters are involved and the problem is too complex. Theories of individual sub-problems with certain boundary conditions are usually developed to fit an aspect of the general problem. Pressure broadening theories are generally classified as statistical or impact theories. Statistical theories are based on the work of Kuhn[44,45] and of Margenau[46-49]. The focus of these theories is on a single molecule perturbed by an average effect of the rest of the system of molecules. This focus does not consider any changes of the molecular interactions in time due to motions of the molecules and, thus, does not

encompass transitions due to collisions. This assumption is only good for very low molecular velocities where intermolecular interaction occurs, and this limitation prevents such a theory from being successful in the microwave region[50]. It was pointed out by Spitzer[51] and Holstein[52] that this approach is valid only in the wings of the microwave lines and at low pressures.

In contrast to the first category, impact theories consider transitions due to collisions. This type of theory has proven to be more successful in the microwave region, especially near the center of the line. The impact theories make certain assumptions that are applied according to the details of the individual problem. These assumptions are:

(1) Impact Approximation: The duration of a collision is short in comparison with the mean time between collisions, which is a valid assumption for pressure less than 1 atm..

(2) Classical Treatment: Wavepackets describing the molecules are well-localized and can be considered point dipoles that follow a definite classical path without a large error.

(3) Binary Collisions: Such collisions result in a perturbation that is proportional to the gas pressure and experimentally fulfilled for low pressures.

(4) Well-Resolved Lines: This is valid for low pressures. However, there is a discrepancy whenever overlapping lines are encountered.

The basis of this type of theory is Lorentz's work[53], but Anderson[54] is usually the name that is associated with it. Anderson's approach follows the general theory of radiation to include both diabatic and adiabatic collisions in the total Hamiltonian. Diabatic collisions cause the transition between energy levels and adiabatic ones do not.

Introducing a time-dependent dipole moment operator, Anderson derived a general expression for the shape of pressure broadened lines :

$$\alpha = \frac{8\pi^2 Nf}{3ckT} |\mu_{ij}|^2 \nu^2 \left[\frac{\Delta\nu}{(\nu-\nu_o-\Delta\nu_o)^2+(\Delta\nu)^2} \right]. \qquad (3)$$

This is the same as equation (2) except for the frequency shift term $\Delta\nu_o$. The shift induced for microwave lines, however, is negligibly small[23], usually of the order of 10^{-2} of $\Delta\nu$, and does not generally affect pressure broadening studies, especially since the line shape is not altered by the shift.

Anderson showed that the linewidth comes from collisions that induce a transition, whereas, the ones that do not induce only the line shift. The derived formulas for the linewidth and the shift for self broadening are:

$$\Delta v = \frac{nv}{2\pi} \sigma_r \tag{4}$$

and

$$\Delta v_o = - \frac{nv}{2\pi} \sigma_i, \tag{5}$$

where n is the number density of molecules, v is the relative mean velocity, σ_r and σ_i are the real and imaginary collision cross sections, respectively. The total cross-section is the sum of the real and the imaginary parts as:

$$\sigma = \sigma_r + i\sigma_i. \tag{6}$$

In order to compute σ, the impact parameter b, the perpendicular distance between the center of the first particle and the incident velocity of the second particle as shown in figure 9, can be defined as:

$$r^2 = b^2 + v^2t^2 \tag{7}$$

This parameter is an important factor in determining what type of collision might take place. For close collisions where r~b, transitions are often induced while for $r \gg b$ they are not. Consequently, in calculating a collision cross-section, σ, some type of weighting factor must be employed in the impact parameter to differentiate between the strengths of various collisions. When we include a weight factor S(b), also called the collision efficiency function, the collision cross-section is evaluated by:

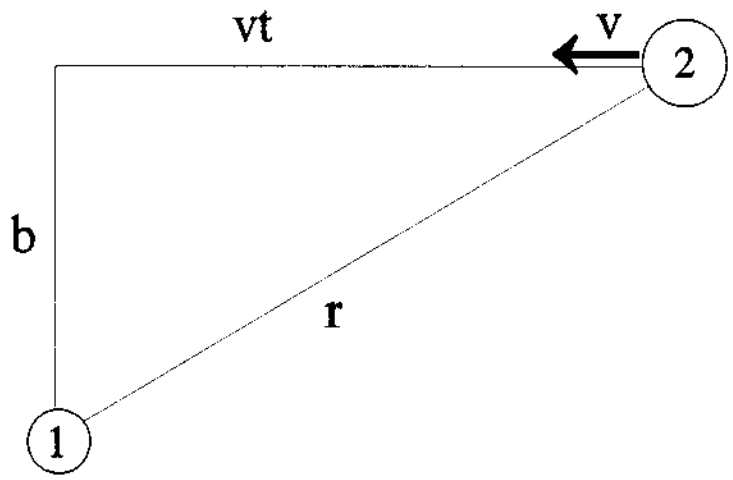

Figure 9. Schematic of a collision between two molecules.

$$\sigma = \int_0^\infty 2\,\pi\,S(b)\,b\,db. \tag{8}$$

In order to evaluate equation (8), S(b) has to be put in a computable form. The very complex preliminary form is simplified by expanding S(b) as:

$$S(b) = S_0(b) + S_1(b) + S_2(b) + \cdots . \tag{9}$$

The terms in the sum are evaluated individually. However, the third term is the one considered, since it is the one responsible for the line broadening. While the first term, $S_0(b)$, corresponds to no interaction and thus can be dropped, the second term, $S_1(b)$, is purely imaginary and contributes only to the line frequency shift which also can be dropped in the line width calculation. Frost[55] has shown that for a pure rotational transition this term is equal to zero. Other terms are simply not considered by Anderson due to the great difficulty in their evaluation and their minimal contribution.

From the previous argument, the weight factor can be put in terms of $S_2(b)$ for the linewidth studies. It also can be simplified by noting that the function has a maximum value of one. The condition for such a value is when the collisions are so strong that their efficiency is 100%. Such collisions require the impact parameter b to be very small and it can have some minimum value such as b_0. For

larger b, the function has to decrease accordingly and this is shown in figure 10. The new simplified function S(b) can be put in the form of:

$$S(b) = \begin{cases} 1 & 0 \le b \le b_0 \\ S_2(b) & b_0 < b. \end{cases} \qquad (10)$$

and the collision cross-section can be evaluated from (8) as:

$$\sigma_r = \pi b_0^2 + \int_{b_0}^{\infty} 2\pi\, b\, S_2(b)\, db. \qquad (11)$$

Even with all of these simplifications, the evaluation of S(b) is still a complicated problem. Since the publication of Anderson's work, a number of authors have worked on other expressions for the weight factor. A general form of the function is given by Birnbaum[25]. Tsao and Curnutte[56] have derived expressions for dipole-dipole, dipole-quadrupole, quadrupole-quadrupole, and dipole-induced dipole inter-molecular potentials. Krishnaji and Srivastava[57,58] have also developed a theory of line broadening.

A rough estimation of the result of Anderson's model for the linewidth can be made as follows: For collisions with $b \ge b_0$, $S_2(b)$ can be put in an approximate form of b^{-m} which makes the weight function as:

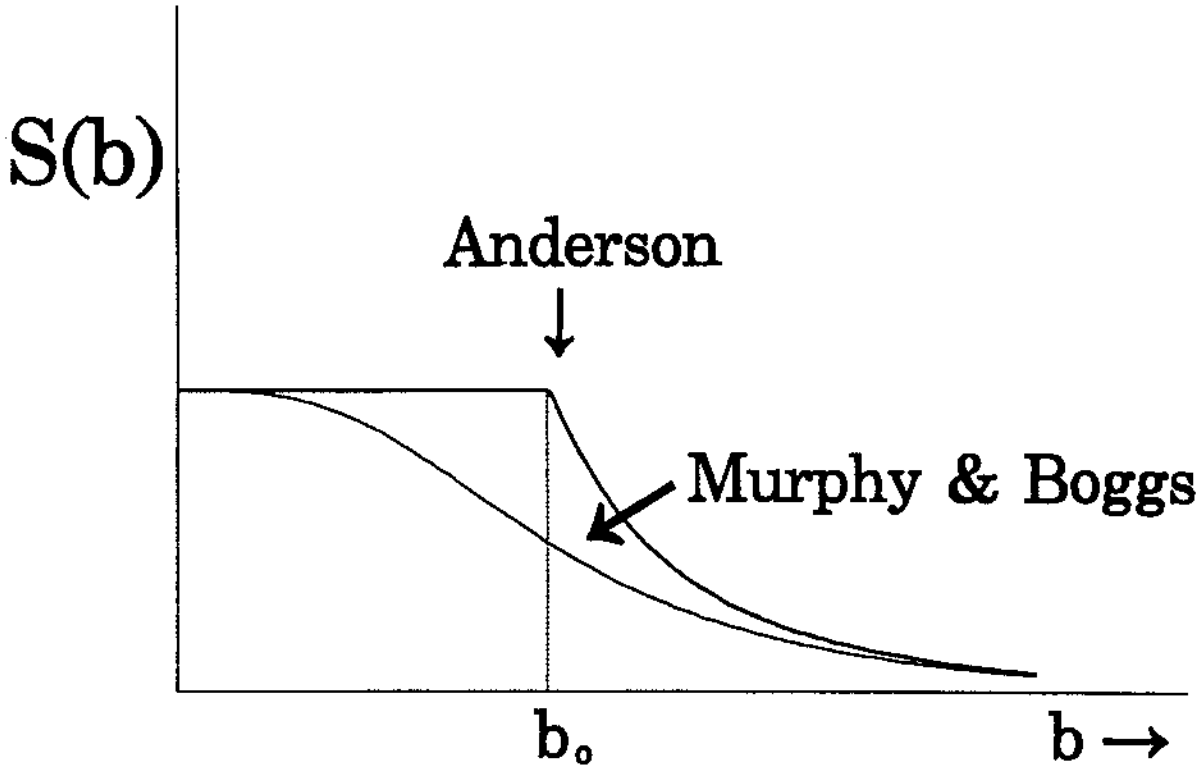

Figure10. A sketch of a collision effeciency function as a function of the impact parameter b in both Anderson and Murphy-Boggs models.

$$S(b) = \begin{cases} 1 & 0 \le b \le b_0 \\ b^{-m} & b_0 < b \end{cases} . \qquad (12)$$

The corresponding linewidth from equation (4) is:

$$\Delta\nu = \begin{cases} \frac{nv}{2} b_0^2 & b \to b_o \\ \frac{nv}{m-2} b_0^2 & b \to \infty \end{cases} . \qquad (13)$$

The lower limit for b, i. e., b_0 can be assumed to be equal to the value of that in the kinetic theory of gases collision diameter r_0. If the interactions are strong, b_0 will be much larger than r_0. For weaker collisions where the impact parameter is small, b_0 has some lower limit such as r_0. The result can be used to evaluate the impact parameter from the kinetic theory as an approximation.

Another result that can be obtained from the model is the evaluation of the dipole moment of an excited state from the linewidth parameter, given that the ground state value is known. Consider the interaction between a molecule in the J_2 state and other molecules of the system. The effective collision-cross section for the molecules in different rotational states is the Boltzmann weighted cross-sections average taken over all these states in which colliding molecules are distributed and that is[59]

$$\sigma_r = \sum_{J_2} \rho_{J_2} \sigma_{J_2} . \qquad (14)$$

where ρ_{J_2} is the fraction of the molecules in the rotational

state J_2. For a rotational transition $J_i \rightarrow J_f$ in a molecule having dipole moment μ_1 colliding with another molecule having dipole moment μ_2, the collision cross-section σ_{J_2} which represent the collisions in the J_2 state, is given by[60]

$$\sigma_{J_2} = \sum_{J_2} \pi \rho_{J_2} b_0^2 \left[1 + \frac{4}{9} \left(\frac{\mu_1 \mu_2}{h\nu} \right)^2 b_0^{-4} \sum_{J_i', J_f', J_2'} D_1 \begin{pmatrix} J_i & J_i' \\ J_f & J_f' \end{pmatrix} D_2 (J_2 J_2') F_1 (k_0) \right], \quad (15)$$

where D_1 and D_2 are the normalized dipole transition matrix elements for the designated transitions. F_1 is a function of $k_0 = (2\pi c/v) b_0 \Delta E$, defined and tabulated elsewhere[56]. The linewidth parameter $\Delta\nu_p$, according to Anderson's theory, given by Eq. (4) is

$$\Delta\nu_p = \frac{n v}{2} \sum_{J_2} \rho_{J_2} b_0^2 \times \left[1 + \frac{4}{9} \left(\frac{\mu_1 \mu_2}{h\nu} \right)^2 b_0^{-4} \sum_{J_i', J_f', J_2'} D_1 \begin{pmatrix} J_i & J_i' \\ J_f & J_f' \end{pmatrix} D_2 (J_2 J_2') F_1 (k_0) \right], \quad (16)$$

where b_0 is determined by the condition

$$\frac{4}{9} \left(\frac{\mu_1 \mu_2}{h\nu} \right)^2 b_0^{-4} \sum_{J_i', J_f', J_2'} D_1 \begin{pmatrix} J_i & J_i' \\ J_f & J_f' \end{pmatrix} D_2 (J_2 J_2') F_1 (k_0) = 1. \quad (17)$$

The linewidth parameter in Eq. (16) becomes

$$\Delta\nu_p = n v \sum_{J_2} \rho_{J_2} b_0^2 \ . \quad (18)$$

Now, the collision impact parameter depends on the dipole moments of the colliding molecules and thus, one can write

$$b_0^2 \propto (|\mu_1||\mu_2|). \tag{19}$$

Substituting Eq. (19) in Eq. (18) one gets

$$\Delta\nu_p \propto \sum_{J_2} \rho_{J_2} |\mu_1||\mu_2| . \tag{20}$$

If the two colliding molecules are of the same species but in different vibrational states, the linewidth parameter of a particular rotational transition in the ground vibrational state can be written as

$$\Delta\nu_{p_0} \propto |\mu_0| \left(\sum_{J_2} \rho_{J_2} |\mu_{J_2}| \right). \tag{21}$$

The linewidth of the same rotational transition in an excited vibrational state v can, likewise, be written as

$$\Delta\nu_{p_v} \propto |\mu_v| \left(\sum_{J_2} \rho_{J_2} |\mu_{J_2}| \right). \tag{22}$$

Dividing Eq. (22) by Eq. (23), one has

$$\frac{\Delta\nu_{p_v}}{\Delta\nu_{p_0}} = \frac{|\mu_v|}{|\mu_0|}. \tag{23}$$

The result in Eq. (23) can be used to scale the dipole moments of a molecule over various vibrational states, provided that the linewidth parameters can be experimentally measured for each vibrational state. The dipole moment for the ground vibrational state can be measured by the conventional Stark shift method.

Linewidths predicted from Anderson's model are often much larger than those observed[58]. Another approach to the

collision function has been developed by Murphy and Boggs[61]. They extended the work of Weisskopf and Wigner[62] and derived an expression for the absorption coefficient similar to that of Anderson. The linewidth and the line shift are calculated with respect to the lifetime of the transition states. If average lifetimes of the initial and final states of the absorbing molecule, averaged over all possible states of the colliding molecules, are τ_i and τ_f , respectively, then the equations for the halfwidth $\Delta\nu$ and the shift $\Delta\nu_0$ are expressed by:

$$\Delta\nu = \frac{1}{4\pi\tau_i} + \frac{1}{4\pi\tau_f}. \qquad (24)$$

$$\Delta\nu_0 = \frac{1}{h}\left[(E_f - E_f^0) - (E_i - E_i^0)\right], \qquad (25)$$

where E_i and E_f are the average perturbed energies of the two states and E_i^0 and E_f^0 are the unperturbed ones. The lifetime of the state J_1 is :

$$\frac{1}{\tau_{J_1}} = \sum_{J_2} \rho_{J_2}\, \Phi(J_1 J_2), \qquad (26)$$

where ρ_{J2} is the density of states in the rotational level J_2. The function $\Phi(J_1, J_2)$ gives the number of transitions per unit time from energy level J_1 due to collisions with molecules in level J_2 and is written as:

$$\Phi(J_1J_2) = 2\pi\int_0^\infty b\ db\int_0^\infty vF(v)\ dv[1-e^{-T_{J_1J_2}(b,v)}], \quad (27)$$

where N is the number of molecules per unit volume, F(v) is the Maxwell-Boltzmann velocity distribution, and b is the impact parameter. The term $T_{J_1J_2}$ is given by:

$$T_{J_1J_2}(b,v) = 2\ S_2(b)_{0,i}, \quad (28)$$

where $S_2(b)_{0,i}$ is Anderson's weight factor. Murphy and Boggs have shown from equation (29) that the linewidth evaluated using their approach is smaller than the those of Anderson and their collision weight factor is also smaller as shown, qualitatively for comparison, in figure 10.

CHAPTER IV

EXPERIMENTAL APPARATUS

The essential task of this investigation is to obtain experimental data and to calculate the line width parameter of selected ν_8 excited vibrational states of ^{13}C tagged CH_3CN. To carry out this goal, the spectrometer used has to be able to measure the widths of these lines over a range of pressure with high accuracy while maintaining the basic requirements such as stability of the equipment, reproducibility of measurements, and high resolution output. These properties are contained in a spectrometer designed by Rinehart[38,63] with some modifications[23].

A new eighth derivative technique was employed in order to recover weak signals and to reduce noise interference. The results proved the effectiveness of this technique in the vibrational components which were measured at room temperature. A block diagram of the spectrometer is shown in figure 11. Details of the spectrometer are subdivided into three parts: radiation source, sample cell, and detection system.

A. Radiation Source

For a stable, tunable, monochromatic radiation, reflex

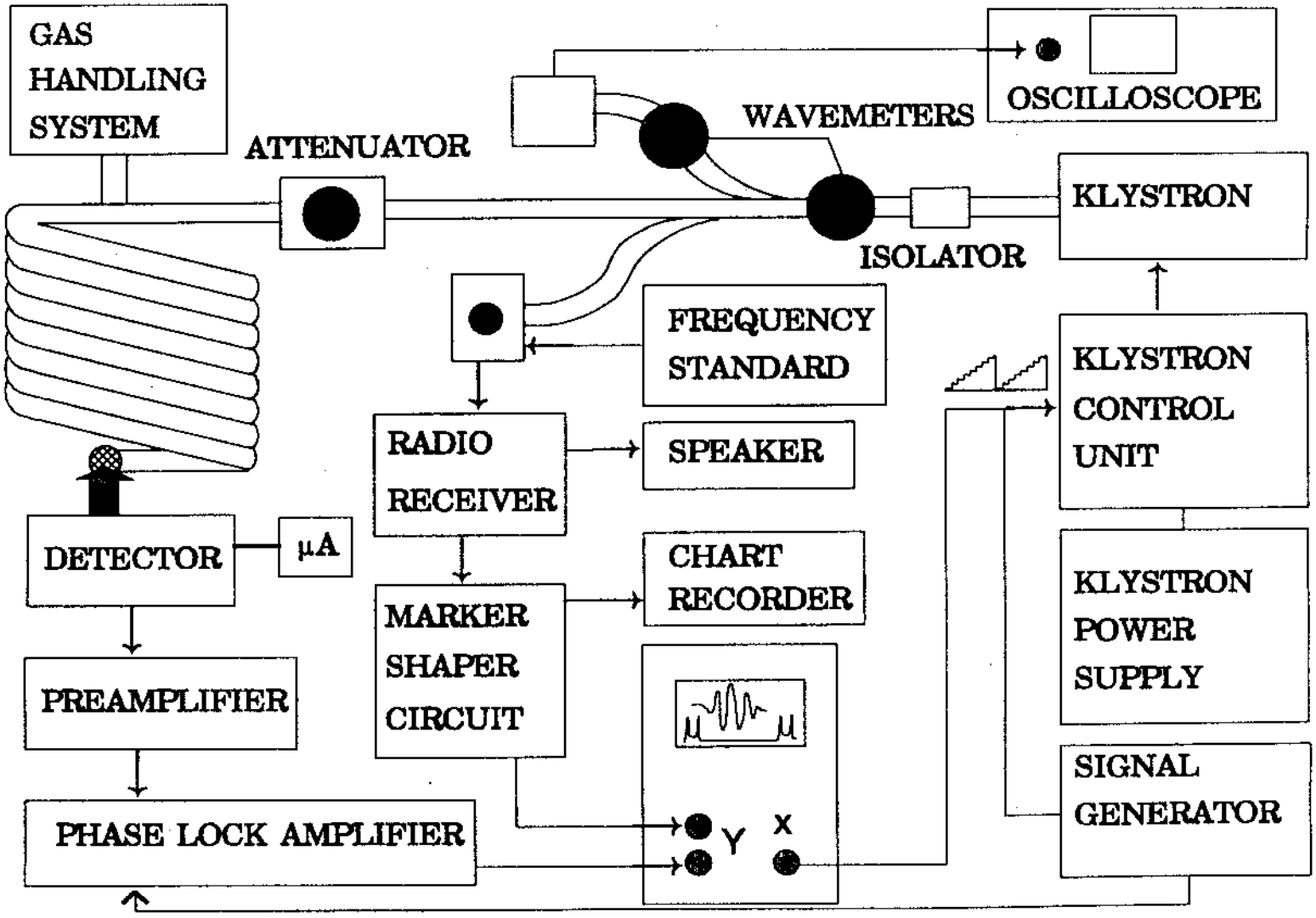

Figure 11. A block diagram of the basic spectrometer used in this work.

klystrons are chosen since they possess such qualities. Selected OKI, Varian, and Cockrill models that provide radiation in the 17-35 Ghz ranges were used. These frequency ranges match the domain of transitions under investigation.

The klystron mean frequency was roughly measured by FXR model Y410A wavemeter or other type, a resonant cavity with a calibrated frequency adjustment, connected with the main guide through a side arm. The absorption signal of the wavemeter was displayed on a Tektronix model RM561A oscilloscope. The power level at the wavemeter was adjusted to give the best absorption signal. Once this was accomplished, frequency adjustments followed and finer frequency measurements were made with a frequency reference circuit.

The frequency of each klystron was adjusted mechanically and electrically. The mechanical adjustment was used while searching for the desired line. This was done by changing the cavity size via a stub attached to the klystron. The size change usually results in large changes in the frequency. Thus, once the range that includes the line was found, electrical adjustments were applied for further tuning. Fine tuning was made by varying the klystron repeller voltage. The dependency of the output frequency on the repeller voltage varies from one klystron to another, but generally it is in the order of one Mhz for

each volt applied.

The sensitivity of the repeller voltage is useful not only for fine tuning the radiation frequency but also in sweeping over a desired range of frequencies. This was done by modulating the klystron with a sweep of voltage ramp obtained from the sweep of the oscilloscope. The modulating was not direct since the ramp voltage (0-180V) was not compatible with the repeller voltage (about 2kV). The necessary voltage transformation was done by a carrier generator modulator circuit. The details of the circuit are given elsewhere[62], but the basic mechanism is as follows: A saw tooth voltage obtained from the time base of a Hickok model 1805A display oscilloscope is mixed with a high frequency of 133.33 kHz square wave. The modulated carrier is sent to a standoff capacitor and into a doubler and demodulator circuit. The recovered sawtooth voltage from the carrier is then impressed upon the klystron repeller. An additional modulation signal was applied to the repeller of the klystron to produce an a. c. signal at the detector of a frequency of 33 kHz. The high Q signal amplifier was tuned at this frequency. The modulation signal was tuned at 33/n kHz as needed for each derivative. The eighth derivative was chosen, therefore n=8.

The klystron high operating voltage was supplied by a Northern Scientific Corporation RE-1610 regulated high voltage (up to 1590V) and a Hamner N4035 high voltage power

supply (up to 3250V). Both have a ripple voltage rating of less than 1mV which makes their noise negligible. The two devices provided the necessary high and well-regulated voltage to the klystron through a control unit.

The daily operation started with turning the power supply for the system on for a few minutes before the klystron to stabilize the supplied voltage. Warm up time of about an hour was allowed for the energized klystron before frequency measurements in order to normalize its power mode. The mode was displayed on a Tetronix model RM561A oscilloscope and adjustments were made, when necessary, to the beam and the operating voltages to minimize line distortion and to center the resonance on the center of the klystron power mode. Once the mode was normalized and the line was at the nearly "flat" center, measurements could be taken. The input power to the cell was controlled by two attenuators placed between the klystron and the cell input window. The attenuators were also preventing reflections in the waveguide system from reaching the klystron and affecting its operation.

B. Absorption Cell

A cylindrical cell with a length of 30.48 m and 0.016 m in diameter was used as the absorption cell. The cell was made of two sections of commercial copper refrigeration

tubing silver soldered together in a smooth joint. The two sections were retained in the coiled configuration in which they were shipped from the vendor. The average diameter of the coils were about 0.53 m.

The cell length is close to the optimum length predicted by Townes and Schawlow[65]. An advantage of such long cells is the increased number of molecules enclosed, which enhances the sensitivity, and thus the increased number of participating molecules absorbing the radiation, which improves the signal to noise ratio.

Teflon vacuum windows were attached to the cell ends to allow changing transition sections of the radiation source and the detector probe without altering the pressure in the cell. Teflon was used for its ruggedness, availability, and its small reflectance, which helps in reducing standing waves. Standing waves, which are unavoidable, were reduced by minimizing the reflection sections and smoothing the joints and the windows of the cell.

Commercial samples of isotopically pure methyl cyanide were obtained from vendors (MSD Isotopes, Division of Merck-Frosst, Canada, Inc., Montreal, Quebec, Canada). Purity rate is 99% for $^{12}CH_3{}^{13}C^{15}N$ and $^{13}CH_3{}^{12}C^{15}N$ and 99.5% for $^{13}CH_3{}^{13}C^{15}N$. The samples were kept pure by freezing them in their reservoirs with liquid Nitrogen baths while pumping out any excess gas via a cold-trap diffusion system. Once the reservoir was evacuated, it was closed and nitrogen baths

were removed. Each sample is kept in an evacuated reservoir until the time of use.

The samples reservoirs were connected to the vacuum pump by a glass connector and to the cell radiation source window by a copper connector. The gas was admitted into the cell rapidly and by small "doses". In order to control the admittance of the gas into the cell, two glass stop cocks in series were used. While the second stop cock was closed, the first one was opened so the gas can fill the space in between the stopcocks and then closed. The second stop cock was then opened as required to allow the gas in the cell. Opening and closing the stop cocks should be done carefully and fast in order to maintain the required pressure level, otherwise more gas will be admitted and the pressure rises beyond the needed range for the experiment.

Pressure in the absorption cell was controlled by an oil vapor diffusion pump cold trapped with liquid Nitrogen forced by a Welch Duo-Seal 1405 mechanical pump. The gas pressure in the cell was measured and monitored by an MKS Baratron 170 M-27D capacitance manometer, factory calibrated. Absolute pressure measurements were assumed to be better than 5 % and relative pressures are assumed to be better than 0.1 %. For each pressure setting a wait of 5 to 15 minutes was taken to allow for pressure stabilization.

C. Detection System

A major concern in conducting the experiment was how sensitive the detecting device had to be to resolve the spectral lines. The line absorption has a low signal strength, $\approx 10^{-10}$ watt, and thus sensitive instrumentation was required. Precise matching of all the spectrometer elements was essential in reducing the standing waves effects. A major enhancement was made by employing a high derivative technique in which a specific derivative of the spectral line rather than its profile is measured. The eighth derivative was chosen so as to recover weak signals of interest and to minimize the standing wave background. The modulation correction of this derivative was high and thus, had to have special consideration in the calculation of the line width parameter. In spite of the need of high modulation, the eighth derivative proved to be very reliable in recovering weak signals and in reducing the distortion of the line due to noise.

Primary signal detection was made by germanium and silicon 1N26 diodes which operate best in the frequency range 10-40 Ghz. A diode was mounted in a rectangular waveguide of cut off frequency well below the line frequency under measurement. The rectangular waveguide was connected, through a transition section, to a short circular copper cylinder that fits into the cell window. To provide maximum

sensitivity and reduce standing waves as much as possible, the detector mount was carefully adjusted by moving the short cylinder in and out of the cell window section and rotating it through a polar angle to reach the best position. A Simpson microammeter connected to the detector to maximize the current was used to monitor the power current and to act as a load on the detector. Once the adjustment was made, the mount was fixed in position by a screw and the current was reduced to about 0.01 μA. The reduction in the current was made to minimize the noise generated in the diode and to prevent line saturation.

The diode output voltage of a few millivolts was amplified by an amplifier-phase sensitive detector set. The signal from the diode is made to pass through a high-Q amplifier tuned at 33 Khz. The tuned amplifier acts as a discriminator to any incoming signal, i. e., it will reject any signal that is not at the tuned frequency. This is useful in allowing the differentiation by a modulation of the signal and in using the nonlinear property of the diode. The power reaching the detector is modulated sinusoidally and the property of the diode produces an output signal that is rich with harmonic components[39] which are an integral number of the frequency of the modulation signal, i. e., the signal output from the diode is:

$$\textit{Signal Output} = \sum_{n=1}^{\infty} (nf_1) \frac{d^n P}{d\nu^n}, \tag{1}$$

where f_1 is the modulation frequency and P is the power of radiation. For the eighth derivative, the output is

$$\textit{Signal Output} = \sum_{n=8}^{\infty} (8f_1) \frac{d^n P}{d\nu^n}. \tag{2}$$

This equation indicates that the frequency of $8f_1$ and higher order integral is admitted since this value is simply the tuned value of the lock-in amplifier. The amplitude of the signal at this high order is small compared with previous ones and thus, a high modulation is required and correction to the modulation is important. The amplitude of the signal of this order (see Appendix C) is given by

$$\rho = 4\gamma P_0 l \left(\frac{\mu_0}{\epsilon_0}\right)^{\frac{1}{2}} \left(p_8^2 + q_8^2 \right)^{\frac{1}{2}}, \tag{3}$$

where

$$p_8 = D \sum_{n=-\infty}^{\infty} J_n \left(\frac{\Delta f}{f_1}\right) J_{n+8} \left(\frac{\Delta f}{f_1}\right) \times \left[\frac{2\Delta\nu + \frac{1}{\Delta\nu}\left[(\nu' + nf_1)^2 + (\nu' + (n+8) f_1)^2\right]}{8\pi^3 \left[\Delta\nu^2 + (\nu' + nf_1)^2\right] \left[\Delta\nu^2 + (\nu' + (n+8) f_1)^2\right]} \right], \tag{4}$$

$$q_8 = (-1)^{-\frac{9}{2}} D \sum_{n=-\infty}^{\infty} J_n\left(\frac{\Delta f}{f_1}\right) J_{n+8}\left(\frac{\Delta f}{f_1}\right) \times \left[\frac{2\Delta\nu + \frac{1}{\Delta\nu}\left[(\nu'+nf_1)^2 + (\nu'+(n+8)f_1)^2\right]}{8\pi^3\left[\Delta\nu^2 + (\nu'+nf_1)^2\right]\left[\Delta\nu^2 + (\nu'+(n+8)f_1)^2\right]}\right], \quad (5)$$

and

$$D = \frac{\pi^2\, \nu_{mn}^2\, f_n\, N\, |\mu_{x_{mn}}|^2}{k\, T\, \tau^2}, \quad (6)$$

with ν_{mn} is the transition frequency between the states n and m.

Next, the signal from the pre-amplifier was sent to a PAR-122 lock-in amplifier used as a phase detector whose reference came from a Heath EUW-27 frequency generator which supplied the modulation. The amplified profile was then displayed on a Hickok model 1805A oscilloscope and recorded by a Rikadinki model RDK B-261 chart recorder.

In order to establish a frequency scale for the line profile, markers were generated by heterodyning the klystron radiation with a known frequency from a General Radio phase-locked standard frequency multiplier set composed of standards suitably locked to a Hewlett Packard quartz oscillator model 105AB checked by comparison with WWV. Beats between the two frequencies, reference and klystron, were detected with a Wells Gardner Radio Receiver BC-348-Q. The beats, heard by a speaker, were shaped by a marker shaper circuit and then sent to the display oscilloscope and to one channel of the dual-pen chart recorder. The position

of these markers was chosen to be 3 MHz apart and positioned in a way that the line profile was in the center. The choice of the interval is to limit errors due to nonlinear effects of the klystron mode. An example of the output of a single line profile with the markers is given in figure 12.

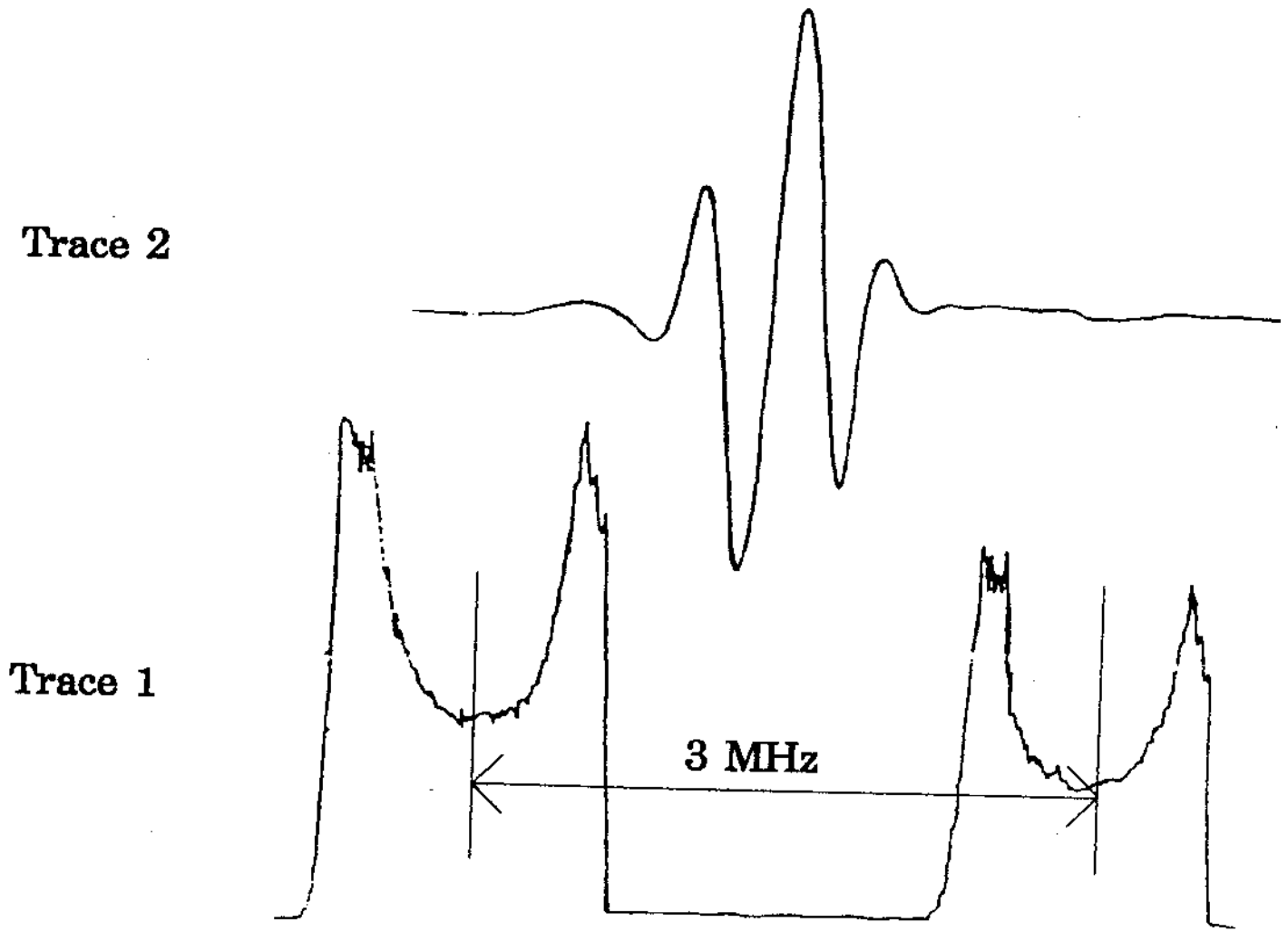

Figure 12. A dual-pen chart recorder output to show a record of a single line. One trace gives the marker interval and the other the line profile.

CHAPTER V

DATA AND ANALYSIS

Investigations of widths of spectral lines require that the width of each line be measured as a function of pressure for a wide range of pressure values so that one can obtain an accurate value of the linewidth parameter for each spectral line. The lines that were investigated in this work are necessarily weak ones. This fact creates a problem. By weak is meant that the intensity of the line is so small as to a degree that make it very difficult to detect and even harder to obtain the profiles over a satisfactory range of pressure to carry out the measurements.

Linewidths parameters of lines identified by frequencies and reported by Tam and Roberts were measured. Schematic diagrams of the energy levels of the ν_8 mode states for $^{13}CH_3C^{15}N$ and $^{13}CH_3{}^{13}C^{15}N$ isotopomers obtained from Tam and Roberts[15] are given in figures (13) and (14).

In the previous chapter, the spectrometer that helped overcome the problem of weak lines and enabled the width measurement to be made was discussed in detail. The enhancements of the hardware and the technique was not, however, the only consideration. In this chapter, the

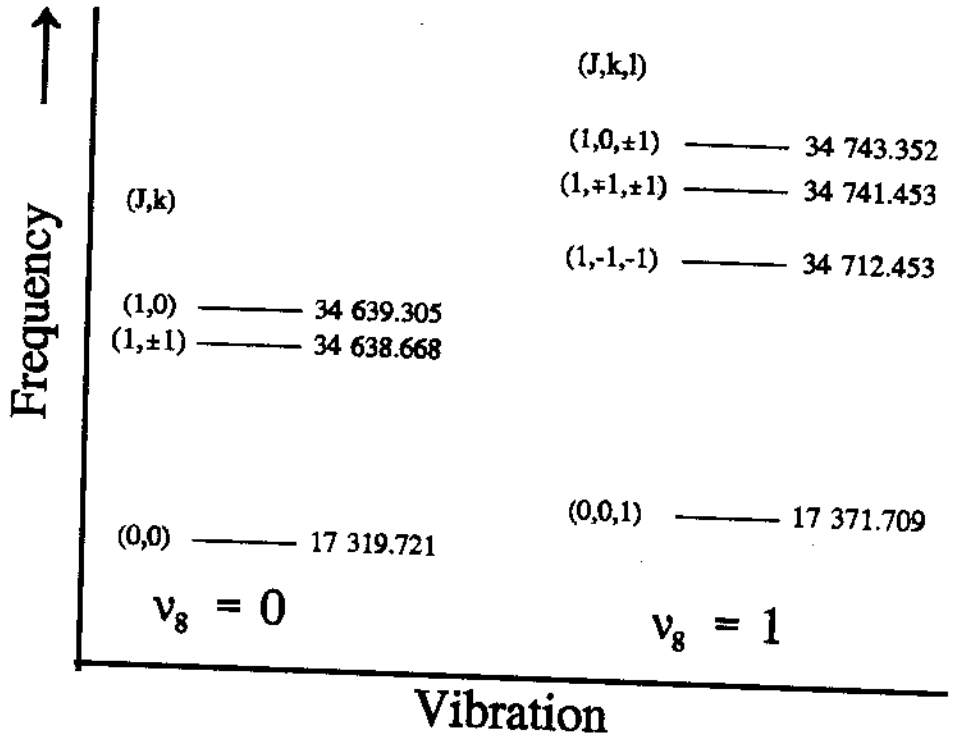

Figure 13. A schematic diagram of the energy levels of the ν_8 vibration for $^{13}CH_3C^{15}N$.

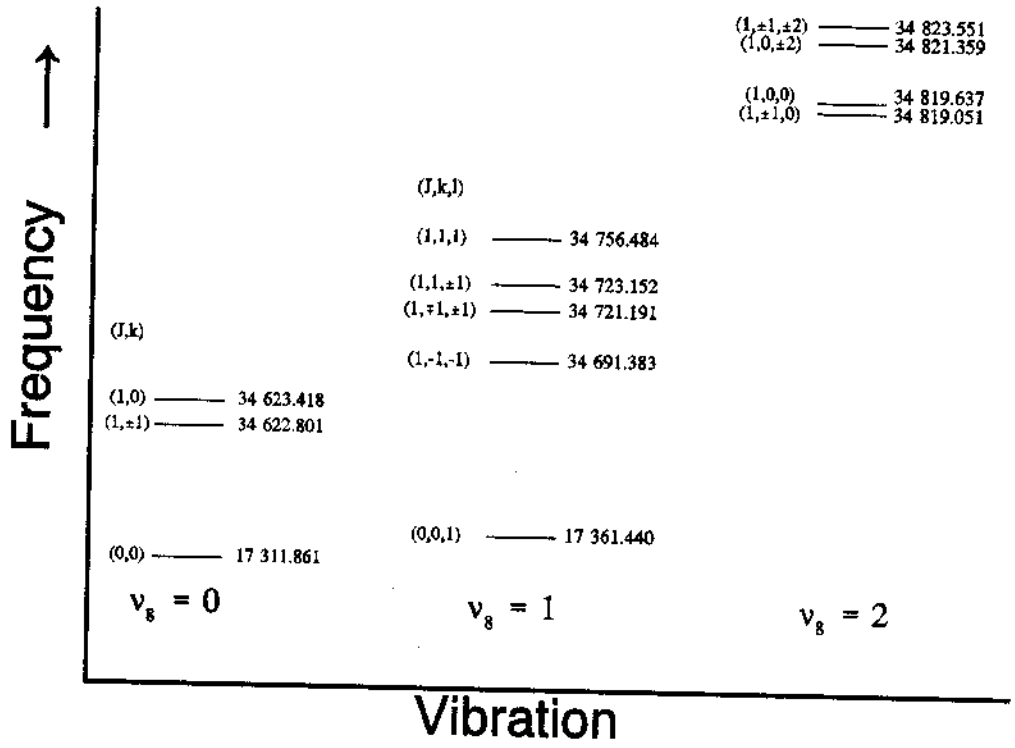

Figure 14. A schematic diagram of the energy levels of the ν_8 vibration for $^{13}CH_3{}^{13}C^{15}N$.

measurements which were carefully taken were subjected to specific tests to see if they should be acceptable for the calculations. These tests are outlined with some details in this chapter.

After tuning the equipments to the working range, the spectral line of a desired state is searched for and detected. Before taking any measurement, the gas was evacuated out of the cell to check if the detected profile is contained for the spectral line only or if it contained same standing wave components, i. e., to determine the nature of the background. The disappearance of the line proves with reduced pressure its nature. Otherwise, it was a profile of some standing waves and the search continue with adjustments of the tuning being made as needed.

Chart records were taken for each spectral line at different pressures after stabilization. The recording for each pressure was repeated from 2 to 7 times so their average could be obtained and thus minimize the errors. Each scan was a check of the previous scan with any irregular signal due to noise disallowed. When the pressure was changed, waiting periods of 5 to 20 minutes were imposed to allow for the pressure to stabilize. The charts were then measured. For each profile, measurements were taken for the "inner" and "outer" peaks in the standard way. The distance between the markers and the splitting of each marker, along with the pressure, were also recorded.

Several tests were applied to the measurements to check the consistency of the data points. According to these tests some data points were disallowed and others were remeasured. It is important to state that this process was based on a physical interpretation and not on how the points are fitted with respect to each other. The tests used were three and in the following discussion some details on each one are given:

1. C/L Ratio Test

The calculation of this ratio depends on the profile whether it is for one line or more:

(i) One Line: C is the distance between the two inner peaks to the line center and L is the distance between the two markers (see Fig. 15). The pattern of this ratio should be linear with some slope since it represent the variation of the width of the line with respect to the pressure.

(ii) Two lines: C in this case is the distance between the line centers. This distance is proportional to the frequency difference between them and hence it should be "constant" in pressure. This assumption is made, in that pressure damping is small enough to be ignored.

Generally, most data points passed this test. Some, however, failed to pass the test. These were either single measurements or their chart records were unclear. Either

way, all points were double checked before its omission or inclusion in the data set.

2. Marker Sweep Test

The markers were set to be at 3 MHz apart. Usually this value was not changed throughout the experiment. On some occasions, the ratio fluctuated slightly due to some nonlinear electronics behavior. The departure from the set value, when it occurred, was checked and usually the errors were due to adjustments.

It is essential that tests were taken for the profiles of more than one line as shown in figure 15. This way the difference between the lines centers in terms of frequency, Δf, was taken as a standard to correct for any irregularity in the markers. The marker interval in terms of frequency was obtained by scaling the marker interval to the known line frequency spacing according to

$$Markers\ (MHz) = \frac{L}{c} \times \Delta f. \qquad (1)$$

The marker test was used only for verification and no points were discarded because of it.

3. Peak's Ratio Test

The inner to the next inner peak's ratio (as shown in figure 16) was used for all the points to check their behavior. The ratios were compared with the corresponding

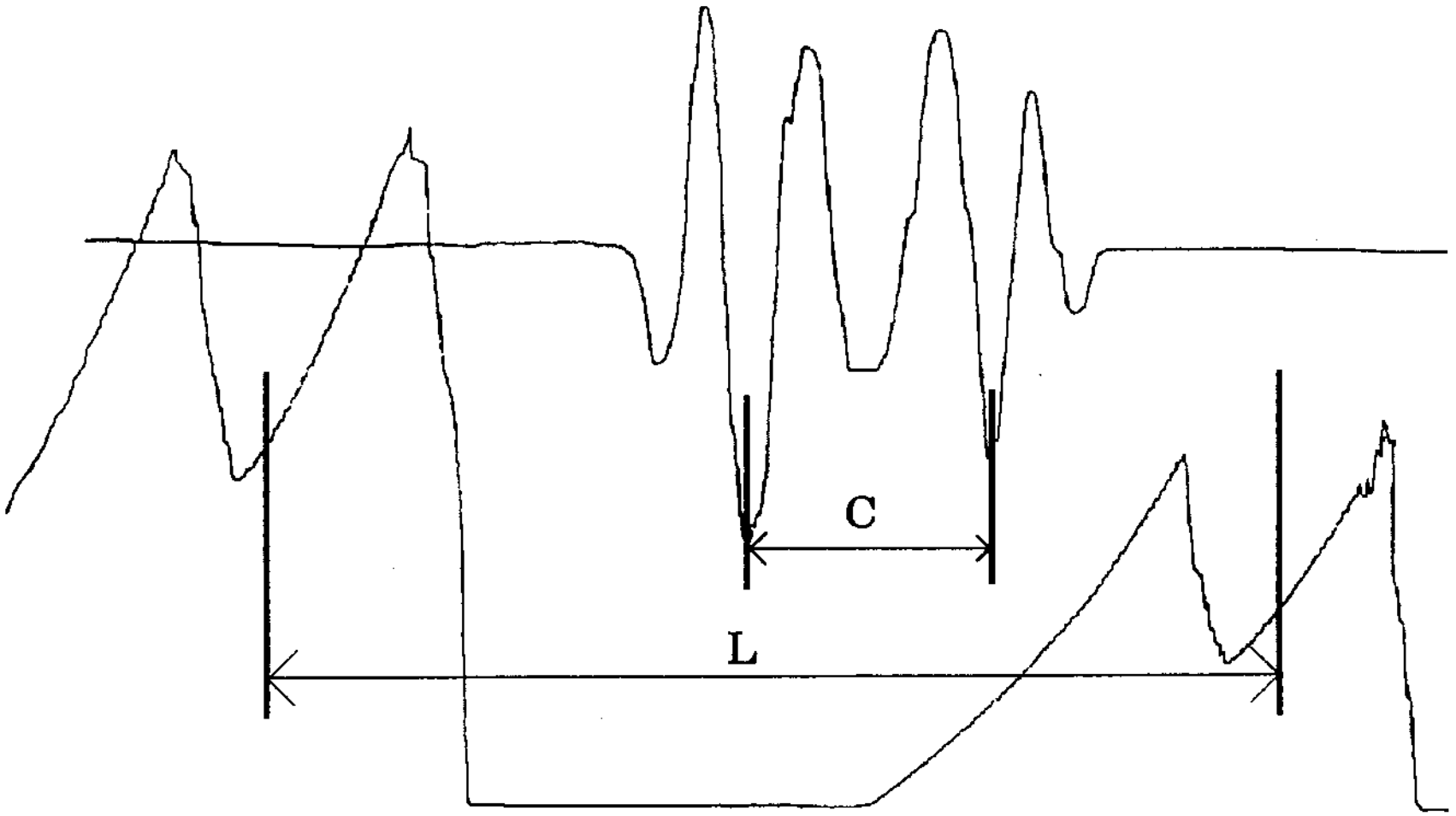

Figure 15. A dual-pen chart recorder trace of the profile of two lines with the markers and parameters C and L shown. The lines appear on one trace and the markers appear on the other.

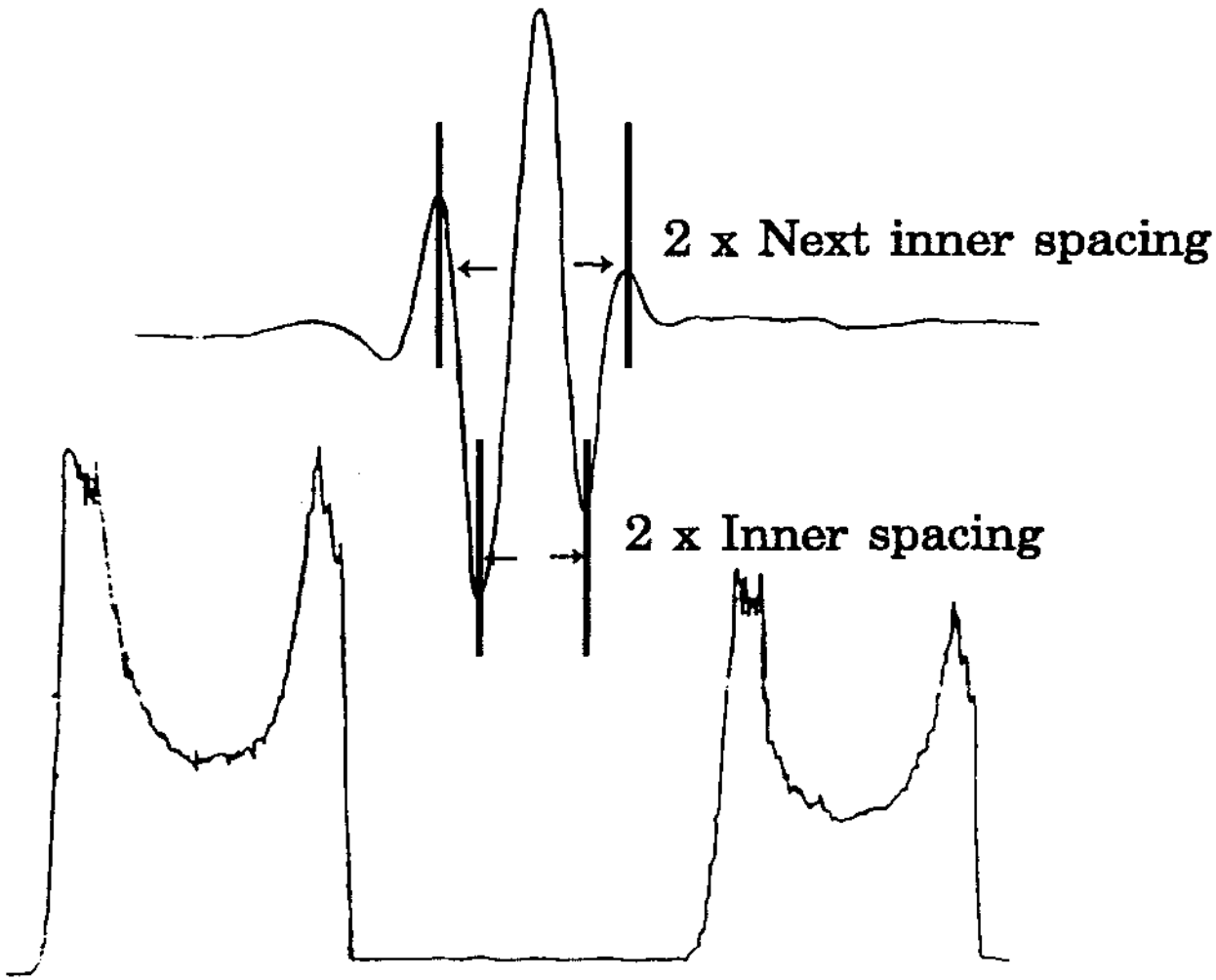

Figure 16. An experimental scan of a dual-pen chart recorder with the inner to the next inner separation spacings are shown.

ratios (figure 4) of the eighth derivative of the Lorentzian function. The test was used to check any irregularity and if found, the measurements of that particular point were redone. In a few cases the points were discarded.

Linewidth Parameter Evaluation

The data points which passed the first and the third tests were corrected for other sources of broadening before applying the pressure model calculations. For source modulation, the correction was based on the model described in chapter II and obtained from equation (17) in chapter II. The modulation broadening of the line was checked by taking the width of a spectral line at fixed pressure and modulation amplitude for 15 runs. The results show a linear trend as shown in figure 17. To find the appropriate parameter for source broadening correction, the method outlined earlier was followed. The measurements of the profile of a spectral line with the pressure stabilized and only the width variation due to the modulation amplitude, were used to plot the width dependence arising due to the amplitude of the modulation. The general relationship was shown experimentally to be linear, as illustrated in figure 18. The slope of the line is simply M which is used in Eq. (17).

The correction due to modulation is the only major one

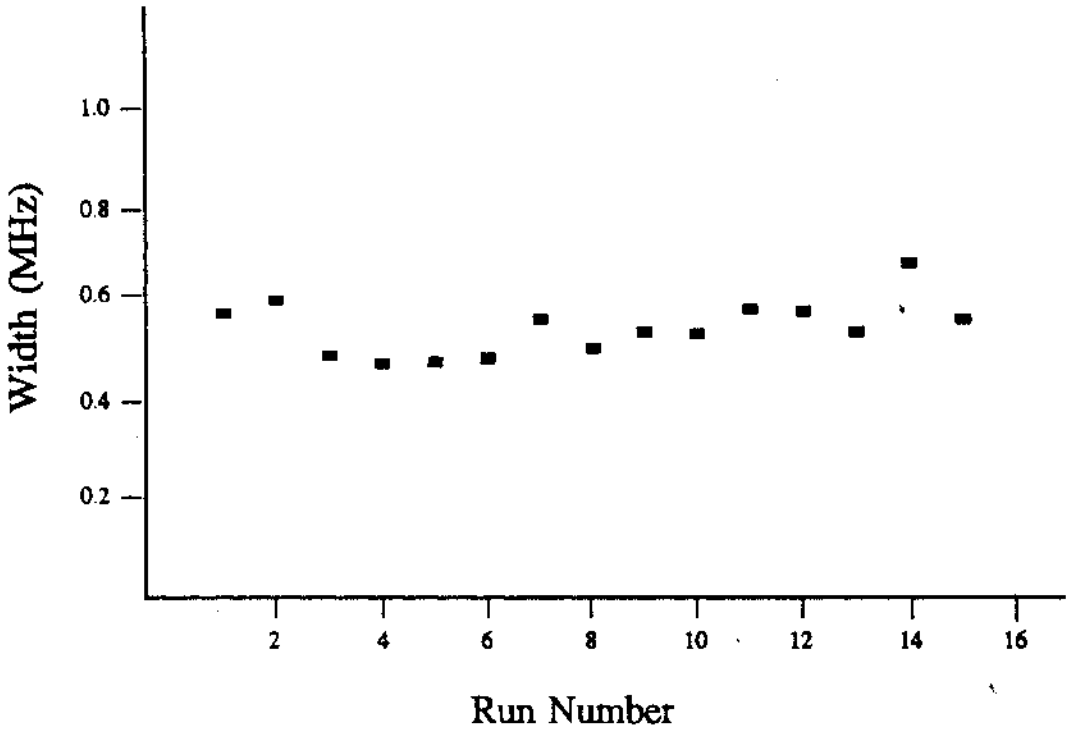

Figure 17. Modulation check of the linewidth for the same modulation at a constant pressure.

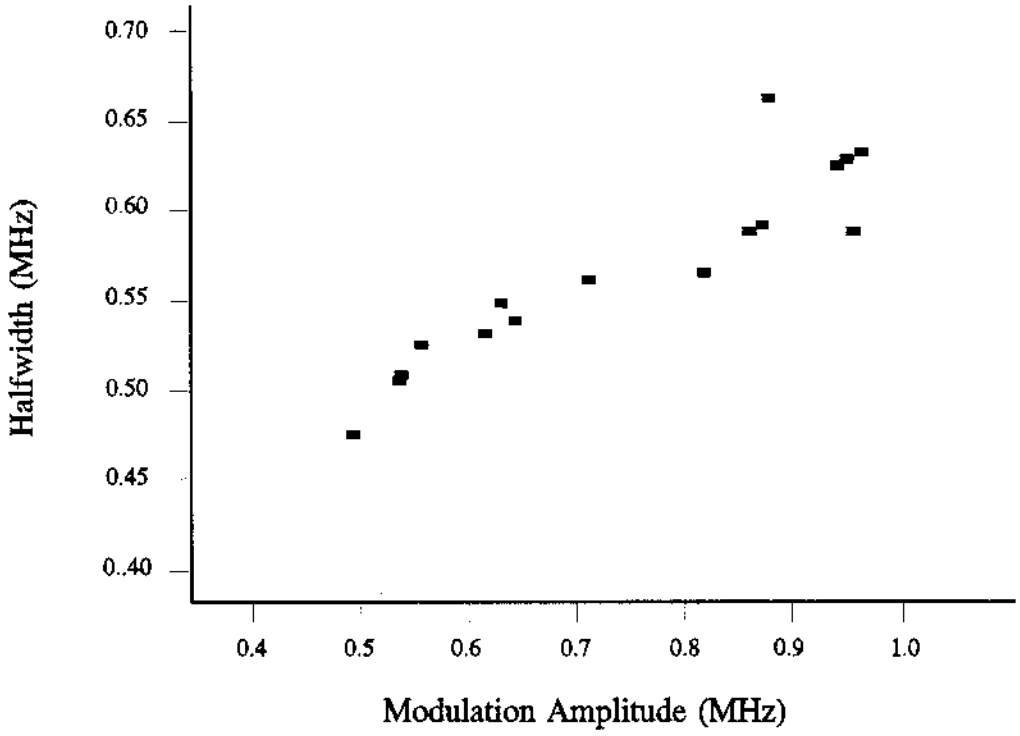

Figure 18. A plot of the experimental half linewidth at half-power-maximum vs. modulation amplitude to obtain modulation correction term M.

after pressure. Doppler broadening to the width was estimated by the equation given earlier in this work for the frequency ranges of the methyl cyanide isotopomers under consideration and found to be around 32 Khz. The cell length broadening was also estimated to be about 2 Khz. Neither of these sources were effective in changing the linewidth parameters due to broadening the lines as their contributions were constant and generally less than the overall experimental errors to the linewidth.

The corrected measured widths were then converted to "true widths", assuming that they obey the Lorentzian model. The correction according to the eighth derivative profile of a Lorentzian shape line is given by;

$$\Delta\nu = \delta\nu_{outer} \times \sqrt{1+\sqrt{.8}} \qquad (2)$$

and

$$\Delta\nu = \frac{\delta\nu_{inner}}{\sqrt{1-\sqrt{.8}}}. \qquad (3)$$

These true widths were averaged and then converted to frequency units in Mhz using the corrected value of the markers interval. This is done according to

$$\Delta\nu(MHz) = \frac{\Delta\nu}{markers\ distance} \times markers\ interval. \qquad (4)$$

The markers interval was 3 Mhz in all the measurements except for the $^{13}CH_3C^{15}N$ ν_8=0, where the interval was 2.288 Mhz. The second value was chosen only for the ground state,

where the intensity is high, and enough to contain the line profile with good resolution. The true linewidths were then plotted against the pressure. By performing a linear least square fit to the data the slope of the line was taken as $\Delta\nu_p$. Some of the plots of the widths versus pressure are given in figures 19, 20, and 21. The calculated linewidth parameters are given in table II. All the measurements were taken for the
transitions from J=1 to J=2 where J is the total angular quantum number and k is the projection of J on the symmetry axis.

The correlation coefficient R^2 is a statistical measure of how well the data points fit a straight line. The values of R^2 show that these lines have linearity between 74% to 95%. Such percentage is a proof of the validity of the technique and correctness of the measurements. The outer to inner ratio refers to the inner and outer peaks distances, respectively. The ratio tests show how these lines compare to a Lorentzian profile. The ratio of the peaks of the eighth derivative is 2.24. The values obtained for these lines indicate that they are 85% to 94% Lorentzian. The deviation from the proposed profile can be partly attributed to minor errors in the measurements. The standing waves can be a factor in this deviation from the expected profile. Another source of distortion can be the overlapping lines. Even though those sources were avoided

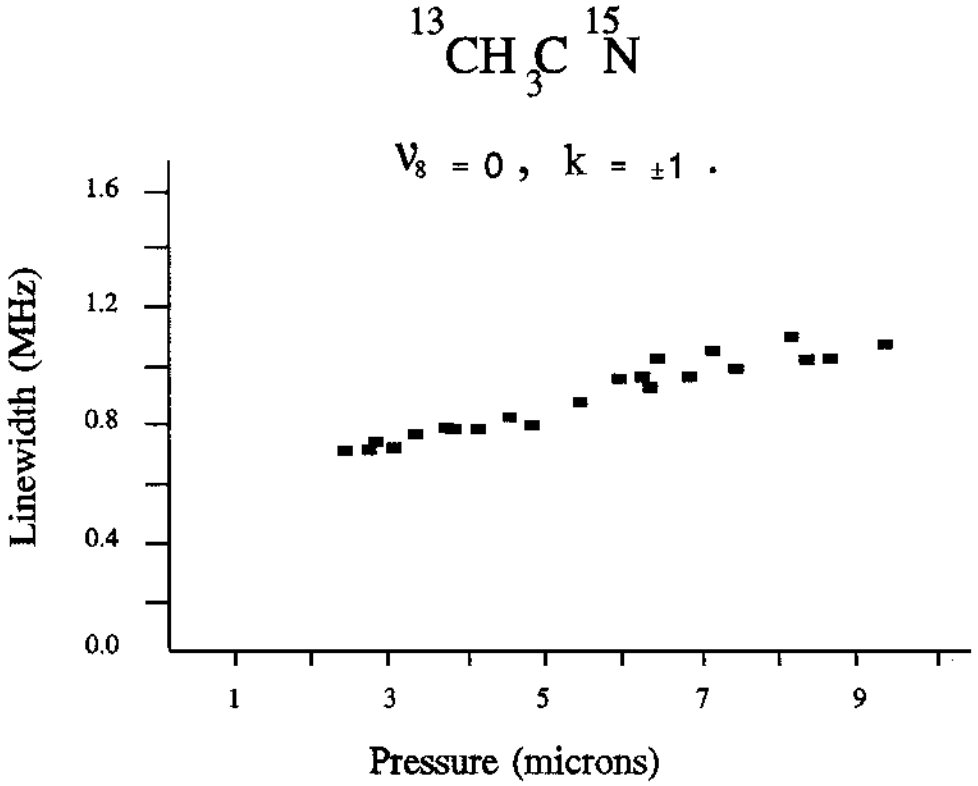

Figure 19. A plot of the linewidth vs. pressure for the $\Delta J=2\leftarrow1$, $k=0, \pm1$, $\ell=0$ rotational components in the ground vibration of the $^{13}CH_3C^{15}N$ molecule.

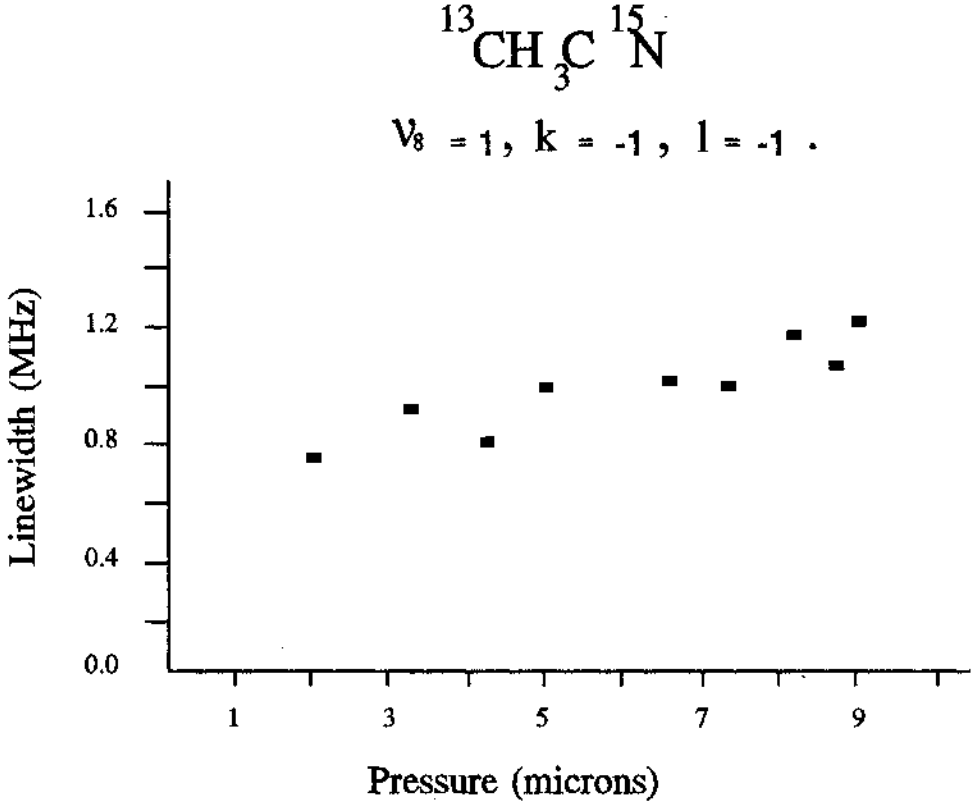

Figure 20. A plot of the linewidth vs pressure for the $\Delta J=2\leftarrow1$, k=-1, $\ell=-1$ rotational components in the first ν_8 vibration of the $^{13}CH_3C^{15}N$ molecule.

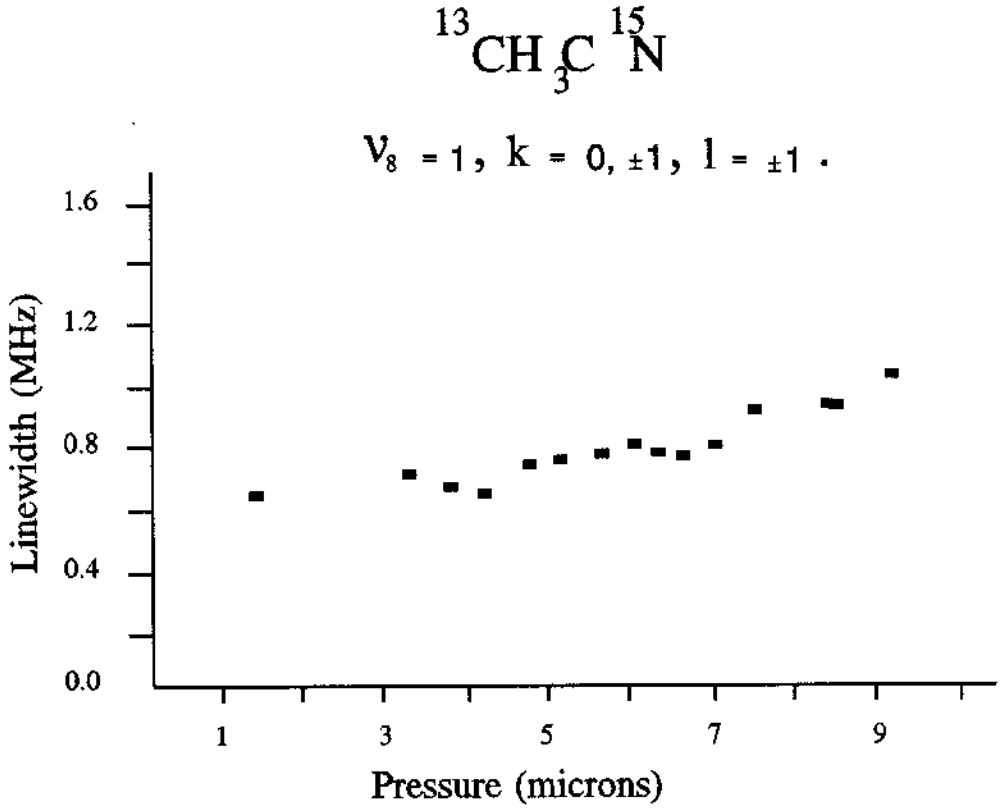

Figure 21. A plot of the linewidth vs pressure for the $\Delta J=2\leftarrow 1$, $k=0, \pm 1$, $\ell=\pm 1$ rotational components in the first ν_8 vibration of the $^{13}CH_3C^{15}N$ molecule.

Table II. A summary of the experimental results for the $\Delta J=2\leftarrow1$ rotational components for $^{13}CH_3{}^{13}C^{15}N$ and $^{13}CH_3C^{15}N$.

Vibration	k	ℓ	$\Delta\nu_p$(Mhz)	R^2	Outer/Inner
$^{13}CH_3{}^{13}C^{15}N$					
Ground	0		71.0±5.1	93%	1.86
ν_8	1				
	-1	-1	50.2±3.4	93%	1.99
	-1	1	50.0±12	76%	1.91
	1	1	48.0±12	75%	1.95
	0	1	46.0±12	74%	2.00
$2\nu_8$	-1	0			
	0	0	53.6±7	87%	1.99
	0	2	50.6±4.3	92%	1.90
	1	0	44.6±2.3	95%	1.99
	1	2	41.2±9	78%	1.90
$^{13}CH_3C^{15}N$					
Ground	1	0			
	1	±1	58.9±3.6	93%	1.90
ν_8	-1	-1	54.9±9.9	82%	1.94
	0	±			
	∓1	±1	45.6±5.2	85%	2.11

as much as possible, they are not removed completely.

Dipole Moment Evaluation

Once the linewidth parameter calculations were completed and the results were assumed satisfactory, they were used to evaluate the dipole moments. For each excited state, the dipole moment was calculated by the formula derived earlier and can be scaled as

$$\mu = \mu_0 \times \frac{\Delta\nu_p}{\Delta\nu_{po}}, \tag{5}$$

where μ_0 and $\Delta\nu_{po}$ are the dipole moment and the linewidth parameter for the ground state with $\Delta\nu_p$ the linewidth parameter of the excited state. The results of the calculations are summarized in table III.

The results have 5% to 26% uncertainty, which is acceptable in this type of study. Part of this percentage comes from the uncertainty of the ground state value of the dipole moment. The value of μ_0=3.92 debye[2] was measured using the conventional Stark cell technique. The dipole moment measurements of the excited states considered in this work could not be measured by the same technique, since they are too weak to be resolved in the Stark technique. The calculation of the dipole moments using the linewidth parameter is a new technique and from the results, it is safe to say that this technique is an alternative for dipole moment determination.

Table III. Results of the dipole moment and the impact parameter calculations for the $\Delta J=2\leftarrow1$ rotational components for $^{13}CH_3{}^{13}C^{15}N$ and $^{13}CH_3C^{15}N$.

Vibration	k	ℓ	μ(D)	P.E.	b(Å)	P.E.*
$^{13}CH_3{}^{13}C^{15}N$						
Ground	0		3.92	7%	28.6	27%
ν_8	1					
	-1	-1	2.77	7%	24.1	26%
	-1	1	2.76	24%	24.0	29%
	1	1	2.65	25%	23.5	50%
	0	1	2.54	26%	23.1	51%
$2\nu_8$	-1	0				
	0	0	2.96	13%	24.9	36%
	0	2	2.79	9%	24.2	29%
	1	0	2.46	5%	22.7	23%
	1	2	2.27	22%	21.8	47%
$^{13}CH_3C^{15}N$						
Ground	1	0				
	1	±1	3.25	6%	25.9	23%
ν_8	-1	-1	3.03	17%	25.0	42%
	0	±				
	∓1	±1	2.52	12%	22.8	34%

* Relative percentage Error.

An interesting feature appears in the calculated values of the dipole moments. This feature is the decrease in their magnitudes as the molecule is promoted to higher excitations. For a bending vibration of the linear part of the molecule, the higher the excited state is, the lower the value of μ. This can be justified according to the definition of the dipole moment in which is $\mu=q\mathbf{l}$ where the q represent the magnitude of one of the charges and l is the distance between them. The moment thus, is proportional to the length of the dipole. In the case of this investigation where ν_8 is under consideration, the excitation means the bending of the C-C≡N bonds which in turn reduces the length of the dipole and that produces a lower value of μ. The results are consistent with the general property of the dipole moment. This is another evidence of the reliability of the method employed.

The induced dipole moment that might alter the energy levels was also calculated to be compared with the permanent moment. The evaluation of the induced moment, μ_i, is based on its definition, i. e.

$$\mu_i = \alpha E, \qquad (6)$$

where α is the polarizability of the matrix element defined as the response of the electron cloud to the external electric field. For methyl cyanide[66] α is on the order of 4.40×10^{-24} cm^3. The ratio of the induced to the permanent

dipole moment is about 3.7×10^{-6}, which means that the induced dipole moment is ineffective when compared to the permanent dipole moment and thus, its effect can be ignored.

Collision Cross-Section

The calculation of the cross-sections is usually presented in terms of the impact parameter which is the minimum distance between colliding molecules. An evaluation for the cross-section using Anderson's model requires a knowledge of the collision efficiency function for methyl cyanide which has not been worked out and thus cannot be used directly for the calculations in this work. The model, however, predicts a lower limit for the impact parameter and that is approximately equal to the kinetic theory hard sphere collision diameter as discussed earlier. The kinetic theory relates the impact parameter to the linewidth parameter (see appendix E) according to

$$b = \sqrt{\Delta\nu_p} \left(\frac{\pi M k T}{4 N_0} \right)^{\frac{1}{4}}, \tag{7}$$

where N_0 is Avogadro's number, k is Boltzmann's constant and T is the temperature. M in the equation is the effective molecular mass of the two colliding molecules and is given by

$$\frac{1}{M} = \frac{1}{M_1} + \frac{1}{M_2}, \tag{8}$$

where M_1 and M_2 are the molecular masses of the two

colliding molecules. In our case, where there was only one type of molecules, often called self-broadening, the effective mass is simply one half of the isotopomer's molecular mass. All units in the calculation are in the MKS system. In order to make the calculation easier for reproduction, Eq. (6) can be put in the numerical form

$$b = \left(\frac{\Delta \nu_p}{0.406} \times \sqrt{M} \right)^{\frac{1}{2}}. \qquad (9)$$

The calculated impact parameters have an uncertainty between 23% and 51%. This is partly due to the nonlinear relationship between the $\Delta\nu_p$ and b. The uncertainty, however, is tolerable since the "hard sphere" model is only an estimation of the impact parameter. More comprehensive models for the impact theory of methyl cyanide may show that the estimation is a reasonable one. The impact parameters calculated are more than twenty times larger than the size of the molecule itself and this indicates how strong the dipole force fields are. Such strengths show that the dipole-dipole interaction is the dominant mechanism of the collision process. The large cross-section also indicates that other forces (such as dipole-quadrupole, quadrupole-quadrupole, etc.) can be safely ignored.

Error Analysis

The range of errors in the measured linewidths is about

5% to 26% for all the lines investigated. The strong lines are assumed to have 5% uncertainty and 26% is assumed for the weak ones. Errors can be from various sources. Standing waves are one of these important sources. It is almost impossible to construct a spectrometer that has no standing waves. The careful adjustments of the different parts of the equipments and the use of a continuous circular cell with minimum flanges helped in reducing the reflection of the power and thus reduced the standing waves but not as much as desired. The major reduction in the effect of standing waves came from the use of the high derivative technique adopted in this work. This technique provided line profiles that do not show the standing waves and thus, seems to minimize their effect. The technique, however, does not get rid of their effect completely, especially for weak lines and that is a cause of errors.

Another source of errors is the overlapping of more than one line when the lines have near lying components. This is true even for a high resolution spectrometer. This is because of the distortion of the profiles by pressure as they get wider and closer to each other. Each line will keep its main profile, but with some distortion because of the presence of the other line.

Some of the klystrons used are very old and noisy and that can contribute to the errors especially for the radiation source broadening. The fluctuation of the

klystron can be a big source of error. These fluctuations are typically due to the effect of the heat on their cavities. While fan-cooling of the klystron helped greatly in reducing the heat effect, it did not completely eliminate the fluctuation.

An important source of errors is the human factor. The chart record has to be read and measured by a ruler. The projected error in the width misreading of 1 mm may be about 10 Khz in the same scans. Add to that the difficulty in determining the precise turning points of some of the weak lines measured and errors due to human intervention become significant. Equipment improvements are being made to enhance the measurements by feeding the results directly into a computer. The data acquisition program that has been developed is not yet reliable enough to do the job. Until the program is perfected the recorded chart reading is the most reliable way to process the data.

Any errors due to frequency shifts were not considered because of two reasons. First, the shift in methyl cyanide spectra is negligible. The second reason is that the shift does not affect the line profile. The only result of this shift is the change in the value of the center frequency and since this is not the topic of this work it was not taken into consideration for measurements.

CHAPTER VI

CONCLUSION

The source modulation spectrometer, with a cell of suitable length, proved to give good signal to noise ratios. The modulation procedure enabled the exploring of the derivatives of the spectral lines. The eighth derivative was chosen so that weak signals could be detected over a reasonable range of pressures. A reliable experimental technique for modulation correction was developed for such high derivatives. The corrected values were used to calculate experimental linewidth parameters. Other parameters were then calculated from the results and used to conclude a picture of the molecular collision mechanism.

The dipole moment values calculated from the linewidth parameters for the excited ν_8 vibrational states are lower than the value for the ground dipole moment. This can be attributed to the fact that the length of the molecule decreases as it bends. The decrease in the first excitation compared to the ground state is 29% for $^{13}CH_3{}^{13}C^{15}N$ while only 17% for $^{13}CH_3C^{15}N$. Comparison with other works for the same molecule is unavailable since no studies on these isotopomers have been made. However, in an experiment on methyl acetylene, another symmetric top, the value obtained

for the dipole moment for the first ν_{10} vibration by Ware et al[59] was 26% lower than the ground value. The value obtained by the present linewidth parameter method for methyl cyanide is significantly lower than that given by Messer et al[67]. obtained from Stark measurements for $CH_3C^{15}N$ isotopomer. The reason for this large difference is not known at this time. However, the use of Stark technique is reliable only for the ground state. The high electric field used in the technique introduces shifts in the energy levels that are much larger than the energy differences between the states themselves. Such effect introduces high uncertainty in the results.

Collision cross sections for vibrationally excited states were obtained from the hard-sphere collision model of the kinetic theory of gases. The values obtained for collision diameters in the ground state were large and do not depart far from that value in the excited vibrational states. These values were not surprising in that the dipole moment for methyl cyanide is about 3.92 D, which would produce such strong long-range interactions.

The source modulation technique proved to eliminate the difficulty of spectral component identification encountered in the standard Stark Modulation spectrometers in which the M components become "blended" into a spectral fan of lines with subsequent difficulty in identification and in establishing the linewidths at half-power maxima. However, the major difficulty seems to be understanding how the

collisional interaction depends on the dipole moments for vibrationally excited states for the molecules.

A work is in preparation to determine the structure of the vibrationally excited molecules of methyl cyanide with ^{12}C, ^{13}C, ^{14}N, and ^{15}N substituted species for a family of molecules of the same chemical composition and dipole moments to determine the trend in structure and the dipole moment for these molecular species. In addition, a computer program which will enable the effect of the background signals to be eliminated from the scan is being developed.

APPENDIX A

Derivation of Lorentz's Formula with the Van Vleck and Weisskopf Correction

Let ω be the angular frequency of the incident radiation and let ω_0 be that of the oscillator whose charge and mass are e and m, respectively. If the electric field is E $\cos\theta$, then the equation of motion is

$$m\left(\frac{d^2x}{dt^2} + \omega_0^2\, x\right) = e\, E \cos(\omega t), \tag{1}$$

with a solution that can be written as

$$x = \Re\left[\frac{eE\, e^{i\omega t}}{m(\omega_0^2-\omega^2)} + C_1 e^{i\omega_0 t} + C_2 e^{-i\omega_0 t}\right]. \tag{2}$$

Where $\Re$ means that only the real part of the expression is to be considered.

If the collision occurs at time $t_0=(t-\theta)$, the transient amplitudes C_1 and C_2 are determined by the values of x and dx/dt immediately after collision. These values are different for different oscillators. Lorentz[26] assumed that positive and negative values of x and dx/dt are equally probable, so that on the average one has $x=(dx/dt)=0$ immediately after a collision. Since the averaging of the polarizations of the various oscillators is a linear process, the net result is the same as that of a single oscillator. This boundary condition is used to solve for C_1 and C_2 and Eq. (2) becomes

$$x = \Re\left[\frac{eE\, e^{i\omega t}}{m(\omega^2-\omega_0^2)}\left[1-\frac{1}{2}\left(1+\frac{\omega}{\omega_0}\right) e^{i\theta(\omega_0-\omega)} - \frac{1}{2}\left(1-\frac{\omega}{\omega_0}\right)e^{-i\theta(\omega_0+\omega)}\right]\right]. \tag{3}$$

To average this expression over the various times of last collision, we multiply by $(1/\tau)e^{-\theta/\tau}$ and integrate over θ from 0 to ∞. Where τ is the mean interval between collisions. the result is

$$x = \Re\left[\frac{eE\,e^{i\omega t}}{m(\omega_0^2-\omega^2)}\left(1-\frac{1+\frac{\omega}{\omega_0}}{2\tau\left[-i(\omega_0-\omega)+\frac{1}{\tau}\right]}-\frac{1-\frac{\omega}{\omega_0}}{2\tau\left[i(\omega+\omega_0)+\frac{1}{\tau}\right]}\right)\right]. \qquad (4)$$

This result fails to reduce to Deby's model, which is a special case (i. e. ω=0). To correct the solution, a new boundary conditions should be considered.

Van Vleck and Weisskopf[27] considered that when solving for the constants C_1 and C_2, the mean distribution for the molecules is affected by the collision and the mean distributions follow the Boltzmann statistics. Their contribution was the application of the Boltzmann distribution law to the Hamiltonian function of the problem which they wrote as

$$H(t) = \left(\frac{p^2}{2m} + \frac{1}{2}m(\omega_0 x)^2 - ex\,E\cos(\omega t), \quad \left(p=m\frac{dx}{dt}\right)\right). \qquad (5)$$

According to the law, the amplitudes C_1 and C_2 after the collision are increased by the amounts ΔC_1 and ΔC_2 such that

$$\Delta C_1 e^{i\omega_0 t_0} = \Delta C_2 e^{-i\omega_0 t_0} = \frac{\int_{-\infty}^{\infty}\int_{-\infty}^{\infty} x e^{-H(t_0)/kT}dxdp}{2\int_{-\infty}^{\infty} e^{-H(t_0)/kT}dxdp} = \frac{eE\cos\omega t_0}{m\omega_0^2}. \qquad (6)$$

the increase to Eq. (3) that come from this is

$$\frac{eE}{m\omega_0^2}\cos(\omega t_0)\cos\omega_0(t-t_0) = \frac{eE}{2m\omega_0^2}\Re\left[e^{i\omega(t-\theta)}\left(e^{i\omega_0\theta}+e^{-i\omega_0\theta}\right)\right]. \qquad (7)$$

Averaging over θ with weighting factor $(1/t)e^{(-\theta/\tau)}$ this becomes

$$\frac{eE}{2m\omega_0^2\tau}\,\Re\left[\,e^{i\omega t}\left(\frac{1}{\left(\frac{1}{\tau}\right) - i(\omega_0-\omega)} + \frac{1}{\left(\frac{1}{\tau}\right) + i(\omega_0+\omega)}\right)\right]. \qquad (8)$$

Adding Eq. (8) to Eq. (4), the corrected solution is

$$x = \Re\left[\frac{eE\,e^{i\omega t}}{m(\omega_0^2-\omega^2)}\left(1 - \frac{\frac{(\omega_0+\omega)\,\omega}{\omega_0^2\tau}}{2\left[\frac{1}{\tau}-i(\omega_0-\omega)\right]} + \frac{\frac{(\omega_0-\omega)\,\omega}{\omega_0^2\tau}}{2\left[\frac{1}{\tau}+i(\omega_0+\omega)\right]}\right)\right]. \qquad (9)$$

If the bracketed factor is written as $Ee^{i\omega t}(x'-ix'')$ the absorption coefficient $\alpha=4\pi N\omega ex''/c$ can be written as

$$\alpha = \frac{2\pi Ne^2}{mc}\left(\frac{\omega}{\omega_0}\right)^2\left[\frac{\frac{1}{\tau}}{(\omega-\omega_0)^2+\left(\frac{1}{\tau}\right)^2} + \frac{\frac{1}{\tau}}{(\omega+\omega_0)^2+\left(\frac{1}{\tau}\right)^2}\right]. \qquad (10)$$

To generalize this result to the general quantum mechanical system, each classical oscillator is replaced with the transition probability between stationary states. The quantum theory[68] of dispersion shows that this can be done by replacing e^2/m with $8\pi^2\nu_0|\mu_{ij}|^2/3h$ and ω by $2\pi\nu$. The ν represent the characteristic frequency associated with a transition between the states i and j and μ_{ij} is the corresponding dipole moment matrix element. The time between collisions τ is replaced by $1/(2\pi\Delta\nu)$, the result of

these substitutions is

$$\alpha = \frac{8N\pi^2}{3ch\nu_0} |\mu_{ij}|^2 \nu^2 \left[\frac{\Delta\nu}{(\nu-\nu_0)^2 + (\Delta\nu)^2} + \frac{\Delta\nu}{(\nu+\nu_0)^2 + (\Delta\nu)^2} \right]. \quad (11)$$

Now, the absorption coefficient is proportional to Δn, the difference in the number of oscillators in the upper and the lower states, i. e.,

$$\Delta n = \left(1 - e^{-\frac{h\nu_0}{kT}} \right) n, \quad (12)$$

where n is the number of molecules per unit volume in the lower state. For the cases where $h\nu_0 \ll kT$, the difference can be approximated by

$$\Delta n = \frac{h\nu_0}{kT} n. \quad (13)$$

The fraction of molecules in the lower state $f=n/\Delta n$ can be used in Eq. (10) to get

$$\alpha = \frac{8N\pi^2 f}{3ckT} |\mu_{ij}|^2 \nu^2 \left[\frac{\Delta\nu}{(\nu-\nu_0)^2 + (\Delta\nu)^2} + \frac{\Delta\nu}{(\nu+\nu_0)^2 + (\Delta\nu)^2} \right]. \quad (14)$$

APPENDIX B

The First Nine Derivatives of a Lorentzian Function and Their Roots

The Lorentz function can be written in a simpler form for the evaluation of the derivatives as:

$$F(x) = \frac{1}{1 + x^2} \tag{1}$$

The first nine derivatives are:

$$F^{(1)}(x) = -2\,x\,F^2 \tag{2}$$

$$F^{(2)}(x) = -2\,[1-3x^2]\,F^3 \tag{3}$$

$$F^{(3)}(x) = 24\,x\,[1-x^2]\,F^4 \tag{4}$$

$$F^{(4)}(x) = 24\,[1-10x^2+5x^4]\,F^5 \tag{5}$$

$$F^{(5)}(x) = -240\,x\,[3-10x^2+3x^4]\,F^6 \tag{6}$$

$$F^{(6)}(x) = -720\,[1-21x^2+35x^4-7x^6]\,F^7 \tag{7}$$

$$F^{(7)}(x) = 40320\,x\,[1-7x^2+7x^4-x^6]\,F^8 \tag{8}$$

$$F^{(8)}(x) = 40320\,[1-36x^2+126x^4-84x^6+9x^8]\,F^9 \tag{9}$$

$$F^{(9)}(x) = -3628800\,x\,[1-12x^2+25.2x^4-12x^6+x^8]\,F^{10} \tag{10}$$

Table IV. The roots of the first nine derivatives of a Lorentzian line

n	Roots				
1	0				
2	$3^{-½}$				
3	0	±1			
4	$\pm(1-0.8^{½})^{½}$	$\pm_{½}(1+0.8^{½})$			
5	0	$\pm3^{-½}$	$\pm3^{½}$		
6	±0.2282	±0.7975	±2.0765		
7	0	±0.4060	±0.9597	±2.4142	
8	±0.1763	$\pm3^{-½}$	±1.1918	±2.7475	
9	0	$\pm(1-0.8^{½})^{½}$	$\pm(1+0.8^{½})^{-½}$	$\pm_{½}(1+0.8^{½})$	$\pm(1-0.8^{½})^{½}$
10	±0.1438	±0.4567	±0.8665	±1.556	±3.4050

APPENDIX C

Coefficients of the Harmonics of the Line Shape as Generated by the Detector

For a molecule in a state n making a transition to the state m at time t_0, the total energy absorbed by all the molecules is given by[39]

$$W(t_0) = \int_0^{\infty} |a_m(t_0)|^2 \left(\frac{h\omega_{mn}}{2\pi}\right) \frac{f_n N}{kT\tau} e^{-\frac{\theta}{\tau}} d\theta. \qquad (1)$$

where $|a_m(t_0)|^2$ is the probability amplitude for the transition, $h\omega_{mn}$ is the energy difference between the two states, N is the total number of molecules, τ is the mean time between collisions, f_n is the fraction of total number of molecules in the state n, k is the Boltzmann constant, and T is the absolute temperature. Eq. (1) can be reduced to the form

$$W(t_0) = \frac{1}{\tau} \int_{\theta=0}^{\infty} \int_{t_0-\theta}^{t_0} e^{-\frac{\theta}{\tau}} \beta(t)\, dt\, d\theta, \qquad (2)$$

where $\beta(t)$ is the rate of energy absorption from the radiation field and expressed by[39]

$$\beta(t) = \sum_{k=-\infty}^{\infty} c_k\, e^{2\pi i k f_1 t}, \qquad (3)$$

where f_1 is the modulation frequency. For a plane wave in the z-direction, the mean value of the poynting vector averaged over an integral number of half cycles, P, can be written as

$$P = \frac{1}{2}\left(\frac{\epsilon_0}{\mu_0}\right)^{\frac{1}{2}} E_0^2, \tag{4}$$

where E_0 is the amplitude of the electric vector of the radiation. From the conservation of energy, this can be put to have the form[39]

$$P = P\, e^{-\alpha z}, \tag{5}$$

where α is the absorption coefficient given by

$$\alpha = 2\left(\frac{\mu_0}{\epsilon_0}\right)^{\frac{1}{2}} \frac{\beta(t)}{E_0^2}. \tag{6}$$

If the radiation is propagated through a layer of gas, the poynting vector at the detector from Eq. (5) can be approximated to $P_0(1-\alpha\ell)$ for $\alpha\ell \ll 1$. The power generated at the detector, $\mathcal{P}$, is proportional to the poynting vector and can be written as

$$\mathcal{P} = \gamma P_0 - 2\gamma P_0 l\left(\frac{\mu_0}{\epsilon_0}\right)^{\frac{1}{2}} \frac{1}{E_0^2}\sum c_k e^{2\pi i k f_1 t}, \tag{7}$$

where γ is the proportionality constant. Since $W(t_0)$ is real, then $c_k = c_k^* = E_0^2(p_k + iq_k)$, where p_k and q_k are defined as the real and imaginary parts of c_k/E_0^2, respectively. Using Fourier expansion for the exponent[39]

$$\frac{1}{E_0^2}\sum c_k e^{2\pi i k f_1 t} = p_0 + 2\sum_{k=1}^{\infty}(p_k \cos 2\pi k f_1 t - q_k \sin 2\pi k f_1 t), \tag{8}$$

and hence, the coefficient of the kth harmonic of the power generated at the crystal is[39]

$$\rho = 4\gamma P_0 l \left(\frac{\mu_0}{\epsilon_0}\right)^{\frac{1}{2}} \left(p_k^2 + q_k^2 \right)^{\frac{1}{2}}. \tag{9}$$

For a sinusoidal frequency modulation, the electric field of the radiation is given by[39]

$$E(t) = E_0 \cos\left(2\pi\nu_0 t + \frac{\Delta f}{f_1}\cos(2\pi f_1 t) \right), \tag{10}$$

where ν_0 is the center frequency, Δf is the amplitude of modulation, and f_1 is the modulation frequency. This expression can be reduced to another form, i. e.

$$E(t) = E_0 \sum_{n=-\infty}^{\infty} J_n\left(\frac{\Delta f}{f_1}\right) \cos 2\pi\left((f_0 + nf_1)\, t + \frac{1}{4} n \right). \tag{11}$$

This expression can be used in evaluating the parameters appearing in Eq. (9). The results can be put in pairs as the following: For even k

$$p_k = (-1)^{-\frac{k}{2}} D \sum_{n=-\infty}^{\infty} J_n\left(\frac{\Delta f}{f_1}\right) J_{n+k}\left(\frac{\Delta f}{f_1}\right) \times \left[\frac{2\Delta\nu + \frac{1}{\Delta\nu}\left[(\nu' + nf_1)^2 + (\nu' + (n+k) f_1)^2 \right]}{8\pi^3 \left[\Delta\nu^2 + (\nu' + nf_1)^2 \right] \left[\Delta\nu^2 + (\nu' + (n+k) f_1)^2 \right]} \right] \tag{12}$$

and

$$q_k = (-1)^{-\frac{k}{2}} D \sum_{n=-\infty}^{\infty} J_n\left(\frac{\Delta f}{f_1}\right) J_{n+k}\left(\frac{\Delta f}{f_1}\right) \times \left[\frac{\left[\frac{(\nu' + nf_1)\,(\nu' + (n+k) f_1)}{\Delta\nu^2} - 1 \right] k f_1}{2\pi \left[\Delta\nu^2 + (\nu' + nf_1)^2 \right] \left[\Delta\nu^2 + (\nu' + (n+k) f_1)^2 \right]} \right] \tag{13}$$

whereas for odd k,

$$p_k=(-1)^{-\frac{k+1}{2}} D\sum_{n=-\infty}^{\infty} J_n\left(\frac{\Delta f}{f_1}\right)J_{n+k}\left(\frac{\Delta f}{f_1}\right) \times\left[\frac{\left[\frac{(\nu'+nf_1)\,(\nu'+(n+k)\,f_1)}{\Delta\nu^2}-1\right]kf_1}{2\pi\,[\Delta\nu^2+(\nu'+nf_1)^2]\,[\Delta\nu^2+(\nu'+(n+k)\,f_1)^2]}\right] \tag{14}$$

and

$$q_k=(-1)^{-\frac{k+1}{2}} D\sum_{n=-\infty}^{\infty} J_n\left(\frac{\Delta f}{f_1}\right)J_{n+k}\left(\frac{\Delta f}{f_1}\right) \times\left[\frac{2\Delta\nu+\frac{1}{\Delta\nu}\left[(\nu'+nf_1)^2+(\nu'+(n+k)\,f_1)^2\right]}{8\pi^3\,[\Delta\nu^2+(\nu'+nf_1)^2]\,[\Delta\nu^2+(\nu'+(n+k)\,f_1)^2]}\right], \tag{15}$$

where

$$D=\frac{\pi^2\,\nu_{mn}^2\,f_n\,N\,|\mu_{x_{mn}}|^2}{k\,T\,\tau^2}, \tag{16}$$

where ν_{mn} is the transition frequency between the states n and m. From Eqs. (15) and (16), the coefficient of the kth harmonic can be found using Eq. (9).

APPENDIX D

Hard Spheres Collision Model of the Kinetic Theory of Gases

In this model, the molecules are treated as smooth, rigid, and elastic spheres of diameter d. When a collision takes place, the centers of the two molecules are a distance d apart as shown in the drawing. If all the molecules are in motion, the collision frequency θ can be written as[69]

$$\theta = \pi d^2 \overline{v_r} n , \tag{1}$$

where v_r represents the average value of the relative velocity of a pair of colliding molecules and n is the molecular density. Using the Maxwell distribution function of molecular velocities, the average molecular speed can be written as[41]

$$\overline{v_r} = \left(\frac{8kT}{\pi m} \right)^{\frac{1}{2}}, \tag{2}$$

where k is the Boltzmann constant, T is the temperature, and m is the effective mass given by

$$\frac{1}{m} = \frac{1}{m_1} + \frac{1}{m_2}. \tag{3}$$

In terms of the mean time between collisions τ, (which is the reciprocal of the collision frequency θ) Eq. (1) can be rewritten with the use of Eq. (2) as

$$\frac{1}{\tau} = \pi n d^2 \left(\frac{8kT}{\pi m} \right)^{\frac{1}{2}}. \tag{4}$$

Now the linewidth $\Delta\nu$ at half maximum is related to the mean time τ by

$$\frac{1}{\tau} = 2\,\pi\,\Delta\nu. \tag{5}$$

Substituting in Eq. (5) in Eq. (4), and writing the diameter in terms of the line width gives

$$d^2 = 2\,\Delta\nu\left(\frac{\pi m}{8kT}\right)^{\frac{1}{2}}. \tag{6}$$

To simplify this equation, m can be replaced by M/N_0 where M is the molecular weight and N_0 is Avogadro's number. The molecular density also can be replaced with N/V where N is the total number of molecules and V is the volume. Making these substitutions, Eq. (6) becomes

$$d^2 = \Delta\nu\left(\frac{\pi MV^2}{2N_0kTN^2}\right)^{\frac{1}{2}}. \tag{7}$$

From the ideal gas formula

$$\frac{V^2}{N^2} = \frac{k^2\,T^2}{P^2}, \tag{8}$$

where P is the pressure. Eq. (7) then becomes

$$d^2 = \frac{\Delta\nu}{P}\left(\frac{\pi MkT}{2N_0}\right)^{\frac{1}{2}}. \tag{9}$$

Anderson's model predicted that the kinetic theory collision diameter can be set to be the lower limit of the impact parameter and that corresponds to $b_0 \approx d$. Approximating the ratio $\Delta\nu/p \approx \Delta\nu_p$, the impact parameter in terms of the linewidth parameter is

$$b_0^2 = \frac{\Delta v}{P}\left(\frac{\pi MkT}{2N_0}\right)^{\frac{1}{2}}. \qquad (10)$$

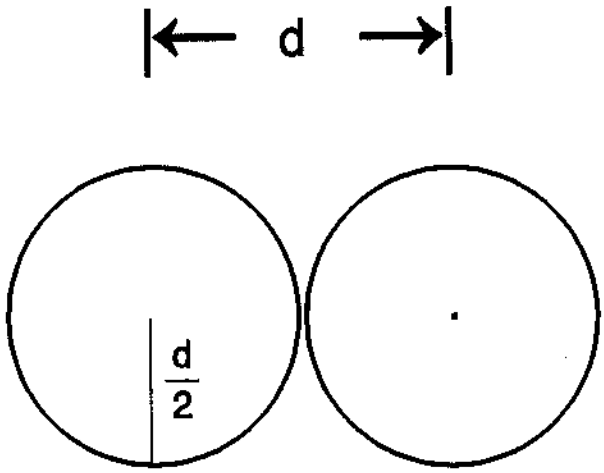

Figure 22. Two spheres of the same radius are in the collision position where the minimum distance between the centers is the sum of their radii or d.

REFERENCES

1. H. S. Tam, Ph.D. Dissertation, (North Texas State University, 1988)115.
2. G. Roussy, Modern Aspects of Microwave Spectroscopy, (Academic Press, 1979)2.
3. H. Rabitz, Ann. Rev. Phys. Chem. 25, 155(1974).
4. E. Herbst and W. Klemperer, Phys. Today 6, 32(1976).
5. M. Al-Share, Ph. D. Dissertation, (University of North Texas, 1990)5.
6. C. H. Townes and A. L. Schawolow, Microwave Spectroscopy, (Dover Publications, Inc. 1975)56.
7. J. L. Duncan, D. C. McKean, F. Tullini, G. D. Nivellini, and J. P. Pena, J. Mol. Spect. 69, 123(1978).
8. D. Boucher, J. Burie, A. Bauer, A. Dubrulle, and J. Demaison, J. Phys. Ref. Data 9, 659(1980).
9. Y. Mori, T. Nakagawa, and K. Kuchitsu, J. Mol. Spect. 104, 388(1984).
10. A. Mito, J. Sakai, and M. Katayama, J. Mol. Spect. 104, 410(1984).
11. F. Sabeh, I. An, W. M. Rhee, and J. A. Roberts, J. Mol. Spect. 125, 348(1987).

12. R. Bocquet, G. Wlodarczak, A. Bauer, and J. Demaison, J. Mol. Spect. 127, 328(1988).

13. F. X. Brown, D. Dangoisse, and J. Demaison, J. Mol. Spect. 129, 483(1988).

14. M. Carlotti, G. Di Lonardo, L. Fusina, and B. Carli, J. Mol. Spect. 129, 314(1988).

15. H. S. Tam and J. A. Roberts, J. Mol. Spect. 134, 281(1989).

16. M. A. Al-Share, J. A. Roberts, and H. S. Tam, J. Mol. Spect. 141, 290(1990).

17. G. K. Johri, M. A. Al-Share, and J. A. Roberts, J. Phys. B: At. Mol. Opt. Phys. 23, 2531(1990).

18. J. A. Roberts, T. K. Tung, and C. C. Lin, J. Chem. Phys. 48, 4046(1968).

19. G.K. Johri and S. L. Srivastava, Nat. Acad. Sci. Lett. 1, 107(1978).

20. D. L. Swindle and J. A. Roberts, J. Mol. Spect. 77, 94(1979).

21. G. K. Johri, R. P. Rishishwar, , A. Kumar, and N. K. Sehgeal, Ind. Jour. pure & appl. Phys. 22, 732(1984).

22. J. K. Messer and J. A. Roberts, J. Mol. Spect. 88 , 231(1981).

23. I. C. Story, V. I. Metchnik, and R. W. Parsons, J. Phys. B: Atom. Mol. Phys. 4, 593(1971).

24. P. Debye, Polar Molecules, (Chemical Catalog Co. Inc.,NY, 1929).

25. G. Birnbaum, Intermolecular Forces, (Interscience Publishers, NY, 1967), 487.

26. H. A. Lorentz, The Theory of Electrons, (Dover, NY, 1909), note 57.

27. H. A. Van Vleck and V. F. Weisskopf, Rev. Mod. Phys. 17, 227(1945).

28. W. Gordy and R. L. Cook, Microwave Molecular Spectra, (John's Wiley and Sons, NY 1970)43.

29. W. H. Ghosh, R. Trombarulo, and W. Gordy, Phys. Rev. 79, 224A(1950).

30. Reference 6, pp. 374.

31. M. Danos and Geshwind, Phys. Rev., 91, 1159-1162.

32. R. Karplus and J. Schwinger, Phys. Rev., 73, 1020(1948).

33. R. H. Schwendeman and H. M. Pickett, J. Mol. Phys., 57, 3511(1972).

34. reference 6, pp. 372-374.

35. T. Oka and T. Shimizu, Phys. Rev. A 2, 587(1970).

36. D. L. Swindle, dissertation, (May 1978)11.

37. R. Karplus, Phys. Rev., 73, 1027(1948).

38. E. A. Rinehart, R. H. Kleen, and C. C. Lin, J. Mol. Spect., 5, 458(1960).

39. R. P. Netterfield, R. W. Parsons, and J. A. Roberts, J. Phys. B: Atom. Mol. Phys. 5, 146(1972).

40. J. D. Jackson, Classical Electrodynamics, (John Wiley & Sons, Inc. 1975)523.

41. F. Reif, Fundamentals of Statistical and Thermal Physics, (McGraw-Hill Co. NY, 1965)268.

42. reference 41, pp. 265.

43. reference 6, pp. 337.

44. H. Kuhn and F. London, Phil. Mag. 18, 983(1934).

45. H. Kuhn, Phil. Mag. 18, 987(1934).

46. H. Margenau, D. T. Warren, Phys. Rev. 51, 748(1937).

47. H. Margenau, Phys. Rev. 48, 755(1935).

48. H. Margenau, Phys. Rev. 76, 121(1949).

49. H. Margenau, Phys. Rev. 82, 156(1951).

50. Reference 6, pp.

51. L. Spitzer, Phys. Rev. 58, 348(1940).

52. T. Holstein, Phys. Rev. 79, 744(1950).

53. H. A. Lorentz, Proc. Amsterdam Acad. 8, 591(1906).

54. P. W. Anderson, Phys. Rev. 76, 647(1949).

55. B. S. Frost, J. Phys. B: Atom. Mol. Phys. 9, 1001(1976).

56. C. T. Tsao and B. Curnutte, J. Quant. Spect. Radiative Trans. 2, 41(1962).

57. Krishnaji and S. L. Srivastava, J. Chem. Phys. 41, 2266(1964).

58. Krishnaji and S. L. Srivastava, J. Chem. Phys. 42, 1456(1965).

59. J. M. Ware, V. Prakash, and J. A. Roberts, J. Mol. Spect. 116, 17(1986).

60. Krishnaji, and V. Prakash, Rev. Mod. Phys. 38, 690(1966).

61. J. S. Murphy and J. E. Boggs, J. Chem Phys. 47, 691(1967).

62. V. W. Weisskopf and E. H. Wigner, Z. Physik 63, 54(1930).

63. E. A. Rinehart, R. L. Legan, and C. C. Lin, Rev. Sci. Inst., 36, 511(1965).

64. J. A. Roberts, Rev. Sci. Inst., 40, 935(1969).

65. Reference 6, pp. 414.

66. D. L. Lide, Handbook of Chemistry and Physics, (CRC press, USA, 1990)10-205.

67. J. K. Messer and J. A. Roberts, J. Mol. Spect. 96, 351(1982).

68. W. Heitler, The Quantum Theory of Radiation, (Oxford University Press, London, 1992)512.

69. R. D. Present, Kinetic Theory of Gases, (McGraw-Hill Book Co. Inc., NY, 1958)30.